AIChE

A Model to Predict Liquid Bridge Formation Between Wet Particles Based on Direct Numerical Simulations

AQ4

Mingqiu Wu and Stefan Radl
Institute of Process and Particle Engineering, Graz University of Technology, Inffeldgasse 13/III, 8010 Graz, Austria

Johannes Khinast
Institute of Process and Particle Engineering and Research Center Pharmaceutical Engineering GmbH, Graz University of Technology, Inffeldgasse 13/III, 8010Graz , Austria

DOI 10.1002/aic.15184
Published online in Wiley Online Library (wileyonlinelibrary.com)

We study dynamic liquid bridge formation, which is relevant for wet granular flows involving highly viscous liquids and short collisions. Specifically, the drainage process of liquid adhering to two identical, non-porous wet particles with difference initial film heights is simulated using Direct Numerical Simulations (DNS). We extract the position of the interface, and define the liquid bridge and its volume by detecting a characteristic neck position. This allows us building a dynamic model for predicting bridge volume, and the liquid remaining on the particle surface. Our model is based on two dimensionless mobility parameters, as well as a dimensionless time scale to describe the filling process. In the present work model parameters were calibrated with DNS data. We find that the proposed model structure is sufficient to collapse all our simulation data, indicating that our model is general enough to describe liquid bridge formation between equally sized particles. © 2016 American Institute of Chemical Engineers *AIChE J*, 00: 000–000, 2016
Keywords: granular flows, wet particles, liquid bridge, liquid transport, direct numerical simulation, volume of fluid method

Introduction

Flow of highly saturated wet granular matter is encountered in a wide range of engineering applications, particularly in the energy sector, or the pharmaceutics and food industry.[1] Due to viscous effects, evaporation or condensation, capillary forces and inhomogeneous liquid distribution in wet granular flows, the liquid transport is difficult to describe and complex flow behaviour is generally observed.[2] Specifically, liquid bridges between particles may lead to particle agglomeration[3] which is either wanted (in the case of wet granulation), or unwanted (e.g., in wet fluidized beds used for coking). Clearly, a better understanding of the formation of liquid bridges will aid in controlling these processes. Previous studies on liquid bridges between particles mainly focused on static bridges,[4] bridge deformation during stretching and rupture,[2,5–7] or the energy dissipated on rupture,[2,8,9] however, few theoretical and experimental studies provided a detailed understanding of the initial bridge formation process, and the accompanying liquid transfer rate from the particle surface into the bridge. Experimental results, and the resulting empirical models, have been summarized by Herminghaus[10], mainly focusing on the effect of roughness, as well as evaporation and re-condensation. Unfortunately, these models cannot be applied to engineering problems, since they (1) focus on the long-term behaviour of the bridge and (2) do not provide a closure for the model parameters.

Studies of liquid bridges between two identical particles were initiated in 1920s[11,12] and were later extended to cover pendular bridges between unequal-sized particles, or a particle and a wall.[4,13] Studies of moving particles and the associated liquid bridge formation were carried out, starting with the work of Pitois et al.[14], which found that the particle relative velocity significantly influences the liquid bridge force. Rossetti and Simons[9] introduced an important improvement, that is, a novel micro force balance device which is capable of observing the liquid bridge between particles and measuring the force exerted by liquid bride. Darabi et al.[2], presented a new coalescence model for binary collision between two identical wet particles, considering capillary and viscous forces exerted by (instantaneously formed) pendular bridges. Despite a variety of researchers[7,15–22] that has broadened our understanding of liquid bridges, a study describing a detailed model on the time evolution of a single (pendular) liquid bridge during its formation phase is still missing. This is due to the lack of our understanding how quickly liquid is transported into a liquid bridge, and how much of the liquid (initially present on the particles) is able to flow into the bridge. One reason for this lack of understanding is that experimental investigations to quantify the liquid present in the bridge are tedious, and that simulations require an enormous spatial and temporal resolution to picture the filling process.

Wet particle collisions, or collisions in a viscous fluid, have been studied by a variety of researchers. For example, Davis

Correspondence concerning this article should be addressed to S. Radl at radl@tugraz.at.

et al.[23], experimentally studied particle collisions with wet smooth surfaces, and they demonstrate that the lubrication forces play an important role on the particle rebound. Donahue et al.[24], further studied the collisions between liquid-coated spheres using a three-body Newton's Cradle, and they revealed that fluid lubrication resistance on rebound plays a key role in the dynamics of the collision. Li et al.[25], calibrated a model with experimental results of wet particle collisions. Gondret et al.[26], focused on the bouncing motion of spherical particles in a viscous fluid, and they quantified the wet restitution coefficient by varying the density and the elastic properties of the solid sphere, as well as liquid film viscosity. Gollwitzer et al.[27], revealed that the dimensionless film thickness is a crucial parameter that affects the restitution coefficient. A rough estimate of the liquid bridge volume, i.e., $V_b \approx {d_p}^3/16$, was used in their work to determine the rupture energy. Sutkar et al.[28] provided a new approach for the estimation of wet restitution coefficients between a particle and a wet surface based on a dimensional and energy budget analysis. However, their data is only in fair agreement with the proposed model, and they have not provided a model for the prediction of the liquid bridge volume. In summary, a large number of researchers have focused on particle collision dynamics without a detailed analysis of liquid bridge formation.[25,29,30]

In this article we focus on applying simulations to elucidate the complex flow processes associated with bridge formation. In general, three categories of simulations methods that aim at modeling liquid bridges can be distinguished: (1) solving the Young-Laplace equation (YLE), (2) solving an approximated version of the YLE based on geometrical simplifications, and (3) a full numerical solution of the Navier-Stokes equation of the gas–liquid systems.

The first approach yields analytical solutions only for certain geometrical configurations,[4] and hence, one has to employ a numerical integration for a general geometrical configuration.[31–33] For example, Lian et al.[32], provided a simple numerical scheme for solving the YLE and revealed that the rupture distance of equally-sized particles can be written as the cube root of the liquid bridge volume for small contact angles. They also obtained a bridge force model based on a simple approximation method, which was independent of the contact angle. Similarly, Mikami et al.[34], and Willett et al.[35], proposed a simple capillary force model by fitting the numerical solution of the YLE. However, as shown in Pepin et al.[8], the drawbacks when solving the YLE to study liquid bridges are that (1) a fixed contact angles is required and (2) that the effect of liquid flow into (or out of) the bridge cannot be predicted.

The second approach is to obtain a simple approximation of the liquid bridge shape, typically by assuming a toroidal[13,36,37] or parabolic shape (see, e.g., Pepin et al.[8]). The benefits of using simplified approximation models are obvious: there is no need to solve the full YLE and an analytical solution can be obtained that can be readily implemented into particles simulation codes. However, approximate solutions become increasingly inaccurate for increasing particle separation[38] and they suffer the same drawbacks as the solution of the YLE.

The third approach is the numerical solution of the Navier-Stokes equations describing (1) the flow of the liquid, or (2) the liquid and the surrounding gas. In the past two decades this approach has been used with increasing frequency. Early research was based on a simplified version of the Navier-Stokes equation, that is, modified boundary conditions were used at the interface (see, e.g., Eggers and Dupont[39] as well as Papageorgiou[40]). Later, Zhang et al.[41], investigated the stretching of a liquid bridge between two circular disks by using a similar method. A fair amount of work to simplify the Navier-Stokes equations for the situation of liquid bridges between two circular disks (but not actual spherical particles) has been performed. Hence, these previous work is only able to provide qualitative information, and has little value for practical application. Only very recently, direct numerical simulations (DNS) of the Navier-Stokes equation have been attempted to simulate liquid bridge formation in an axisymmetric setup.[42–45] These methods provide a full description of the liquid bridge dynamics, and hence are a promising approach for studying the bridge formation process.

Objectives

Only few theoretical and experimental studies in the literature were concerned with the bridge formation process and the accompanying liquid transfer rate into the bridge. While models for liquid transfer on bridge rupture exist Lian et al.[32], as well as Shi and McCarthy[46], these models still require additional assumptions for the liquid volume present in the bridge. With this in mind, we have started investigations to establish a detailed model that is able to predict liquid transport and the distribution of liquid between two spheres in our recent work.[43] In the present work, we systematically study the liquid bridge and drainage process of liquid adhering to two identical wet particles. We use a DNS based on the Volume of Fluid (VoF) method, that is, we simulate both the motion of the liquid and the surrounding gas. By reconstructing the interface between these two fluid phases, we extract the interface position to identify the bridge shape and size. Specifically, the liquid bridge is defined by detecting the neck positions of the liquid film on each particle surface (for details see the "Liquid Bridge Volume calculation" section). We then use a direct integration method (DIM) to calculate the liquid bridge volume based on the interface position at each instant in time. Our ultimate goal is then building a dynamic model for the liquid bridge volume during the filling process based on these DNS data. Therefore, we fit our DNS data to a postulated liquid bridge filling model, which is an extension of the ideas of Mohan et al.[47], but still allows for an analytical solution to predict the bridge volume. Specifically, our postulated model assumes that the filling rate is not affected by the particles' relative motion, and that the filling rate is linear in the difference between the liquid present on a particle and the bridge volume. Such a model requires the specification of only three dimensionless parameters, as we will show in the following. While our work is currently limited to smooth particles of identical size, the model proposed by us can be easily re-calibrated to account for, that is, particle roughness, or particle size differences once data for the amount of liquid in the bridge is available for these situations.

In the following, we first describe the methodology used to establish the liquid bridge model, including (1) the initial bridge and boundary conditions that have been used in our simulations, (2) the interface feature extraction procedure, as well as (3) the postulated model itself. Subsequently, we introduce a geometrical bridge volume, which is used to normalize the bridge volume measured from our detailed simulations. Then we present results, starting with the calibration of the sub-models for the initial bridge volume and the subsequent viscous filling stage, and we are the first to provide a dynamic

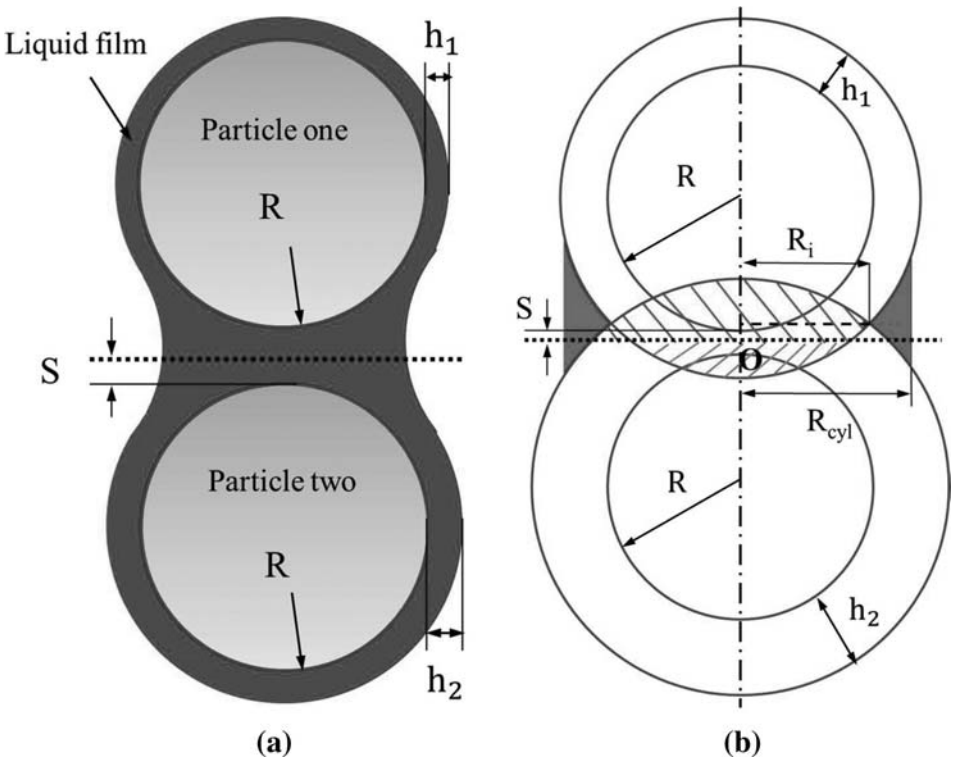

Figure 1. Sketch of the simulation setup, as well as the initial bridge shape.

[Color figure can be viewed in the online issue, which is available at wileyonlinelibrary.com.]

model for predicting liquid bridge formation. Also, the effect of grid refinement, as well as that of the Reynolds number, are carefully analyzed as well. Finally, we discuss our findings and provide conclusions that should guide the application and future extension of our model.

Methodology

Initial and boundary conditions

We consider two identical smooth spheres, which are fixed in space, that is, the spheres' relative velocity is zero. In this work, we consider the general situation of an asymmetric liquid bridge, that is, the thickness of the films initially present on the particle surfaces are different. In what follows, we define that particle 1 always has less liquid compared to particle 2, as shown in Figure 1 (panel a). R is the sphere radius for two particles, and h_1 and h_2 are the initial film heights of particle 1 and particle 2, respectively. S is defined as the half separation distance between the particle surfaces.

The initial shape of the liquid bridge has been set according to the initial film height and the particle separation. Because we do not simulate the approach of the spheres, and hence cannot predict the deformation of the liquid films on the particle prior to coalescence, we must assume the initial bridge shape right after the films have coalesced. Specifically, we assume that the liquid in the overlapping region of the liquid films (i.e., red and green shaded regions in Figure 1b) is instantaneously displaced laterally, and flows into a ring-shaped region. The latter is illustrated by the red solid area in Figure 1b, that is, the bridge has been considered to be cylindrical at time zero. Geometrical considerations, discussed in greater detail in "Geometrical Bridge Volume" section, can now be used to predict the size of the ring-shaped region. These considerations, as well as the assumption of zero initial velocity and uniform pressure distribution, have been used to initialize all our simulations.

Most important, in our simulations there is no gravity, or other force acting on the system. The physical reason why liquid in the films on the particle surfaces flows into the liquid bridge is as follows: the pressure in the film (adhering to the particle surface, and far away from the bridge) can be estimated as $p_s \approx 2\sigma/R$, while the pressure in the liquid bridge region can be approximated as $p_{V_b} \approx -\sigma/R_{\text{curve}}$. Here R_{curve} is the radius of curvature of the liquid bridge surface. Thus, the pressure in the liquid bridge region is always negative or zero, while that in the film is always positive. Hence, a pressure difference between the particle surface and the liquid bridge region exists, driving the liquid into the bridge. This liquid flow will not stop until the pressure difference reaches zero, or the liquid film on the particle surface ruptures (for details about film rupture see section "Film Rupture and Grid Refinement").

VoF simulation approach

A VoF method,[48] which is available as "interFoam" solver in the open-source software package OpenFOAM®, has been employed in our simulation. The interFoam solver has been verified extensively by Deshpande et al.[48], and we have also made several tests, for example, calculating the pressure distribution in a liquid film coating a single sphere. For a typical grid resolution of $\Delta h = \Delta x/h_1 = 0.10$ (here Δx is the grid spacing, and h is the film height), these test show that the pressure can be predicted within an acceptable error tolerance of ca. -4.6%. In addition, we have tested the grid dependency of our results, and found that $\Delta h = 0.12$ gives acceptable results for most situations of interest (see section "Film Rupture and Grid Refinement" for more details).

Another critical point when it comes to two-phase flows is the prediction of the dynamic contact angle, since this is not a constant, but is influenced by the speed of the three-phase contact line. Unfortunately, the current implementation of dynamic contact angles in the "interFoam" solver has not been verified, and hence we are unable to accurately simulate the motion of three-phase contact lines. However, we have spared out this detailed by simply assuming that the spheres are completely coated, and hence there is (initially) no three-phase contact line in our simulations. This allows us to apply the "interFoam" solver for our studies of two coated particles without additional modifications. It must be mentioned here that for long times we observe a rupture of the liquid film present on the spheres. In such a situation a three-phase contact line forms, and hence, our solver will deliver inaccurate (but still physical) predictions of the liquid bridge shape after rupture. We accept this inaccuracy for the time being, and simply have not considered data collected after film rupturing events in our analysis.

The transport equation for a color function, representing the volume fraction of the liquid phase, is solved together with the continuity and momentum equations:

$$\frac{\partial(\rho \boldsymbol{U})}{\partial t}+\nabla\cdot(\rho \boldsymbol{U}\boldsymbol{U})=-\nabla p+\mu\left[\nabla \boldsymbol{U}+(\nabla \boldsymbol{U})^T\right]+\boldsymbol{f}_b \quad (1)$$

$$\nabla\cdot \boldsymbol{U}=0 \quad (2)$$

$$\frac{\partial \alpha}{\partial t}+\nabla\cdot(\boldsymbol{U}\alpha)=0 \quad (3)$$

where $\boldsymbol{U}$ is the velocity field shared by the two fluids (i.e., the liquid on the spheres and the surrounding gas) throughout the flow domain, and α is the phase fraction indicator. ρ is density, p is pressure, and f_b are body forces, which include (1) surface tension effects at the interface, and (2) gravity. However, effects due to gravity have been neglected in our simulation, because viscous and capillary effects are dominant in situations involving relevant particles (i.e., in situations in which particles have a diameter that is smaller than the capillary length). The phase function αcan proceed within the range $0<\alpha<1$, with alpha being zero (or unity) in regions occupied by the gas (or the liquid), respectively.

The physical properties are computed as averages based on the distribution of the liquid volume fraction α. Specifically, we use:

$$\rho=\rho_l\alpha+\rho_g(1-\alpha) \quad (4)$$

$$\mu=\mu_l\alpha+\mu_g(1-\alpha) \quad (5)$$

where ρ_l (or μ_l) and ρ_g(or μ_g) are the density (or the dynamic viscosity) of the liquid and gas, respectively.

Relevant dimensionless quantities describing the problem can be readily identified: the dimensionless initial film heights, the dimensionless separation distance, the bridge volume and the amount of liquid on particle surface normalized by a reference volume (i.e., the particle radius cubed R^3), the density and viscosity ratio between the liquid and the ambient gas, the pressure scaled with a typical capillary pressure (i.e., surface tension over the particle radius) and the velocity scaled with a typical capillary speed (i.e., the ratio of surface tension and viscosity of the liquid). The relevant time scale can be based on a corresponding viscous time scale, which is chosen to be the ratio of the particle radius and the capillary speed. Finally, we may want to consider the effect of the fluid's inertia on the filling process, and hence a Reynolds number can be defined based on the capillary speed, the particle radius, and the fluid viscosity. Note, that alternatively an Ohnesorge number can be defined, with is simply the inverse of the square root of the Reynolds number as summarized below:

- $h_1^+=h_1/R$, $h_2^+=h_2/R$, $h_0^+=\left(h_1^+ +h_2^+\right)/2$, $S^+=S/R$;
- $L_{p1}^+=L_{p1}/R^3$, $L_{p2}^+=L_{p2}/R^3$, $V_b^+=V_b/R^3$;
- $\rho_{\text{ratio}}=\rho_l/\rho_g$, $\mu_{\text{ratio}}=\mu_l/\mu_g$;
- $u_{\text{ref}}=\sigma/\mu_l$,$p_{\text{ref}}=\sigma/R$, $t_{\text{ref}}=R\mu_l/\sigma$;
- $t^+=t/t_{\text{ref}}$
- $\text{Re}=\sigma R\rho_l/\mu_l^2$, $Oh=\mu_l/\sqrt{\rho_l\sigma R}=1/\sqrt{\text{Re}}$, $Ca=\mu_l|U|/\sigma$.

A typical result of our DNS is shown in Figure 2, in which we illustrate the dimensionless flow velocity for various dimensionless times. Most important, this figure illustrates that the dimensionless velocity strongly decrease with time, and it can be expected that the rate with which the bridge is filled decreases with increasing time. F2

All relevant simulation parameters and numerical scheme are defined in Table 1. T1

Liquid bridge volume calculation

The gas–liquid interface can be easily determined from the DNS data by analyzing the distribution of the phase fraction. Hence, we have taken a simple, yet effective sampling method to detect the gas–liquid of the film and the bridge formed between the particles.

As can be seen in Figure 3, the sampling procedure takes place between O_1 and O_2 with an interval of δx and a large enough sample distance in the y-direction. By applying the sampling interval from O_1 and O_2, we obtain a list of data for the phase value along each sampling line, and consequently the interface position can be determined at $\alpha=0.5$. F3

Next, we need to define which portion of the fluid in the system is considered to be in the liquid bridge. As can be seen from Figures 2 and 3 (panel b), there exists a minimal liquid film thickness on each of the two spheres. Thus, if one would analyze the thickness profile on each particle, one can observe a certain angular position where the film is thinnest. We have used this local minimum to define the extent of the liquid bridge. Specifically, we denote these positions of the minima as the "neck" positions, which separate the bridge from the film adhering to the particle surface. These neck positions are the basis for the subsequent bridge volume calculation.

After the interface positions and neck position have been determined, we can calculate the liquid bridge volume by using a DIM. Specifically, we use slices with thickness δx (see Figure 3, panel b), as well as the known neck positions, to determine the bridge volume by numerical integration using the trapezoidal rule.

Proposed model for liquid bridge filling

Our DNS indicate that the mechanism of liquid bridge formation consists of the following steps: after the coated particles get close to each other (caused by the relative motion in a real-world granular flow), the films coalesce, a liquid bridge is then formed between the particles, and finally liquid drains into the bridge. Thus, it is reasonable to assume that there is (1) a very fast initial formation processes (immediately after coalescence; since we cannot resolve this process, we will simply assume a certain initial bridge volume), and (2) and a comparably slow filling process. Consequently, we differentiate between two stages of the filling process of liquid bridge: (I) a capillary-force driven initial stage (fast filling), and (II) a viscous filling stage (slower filling). Although these two stages

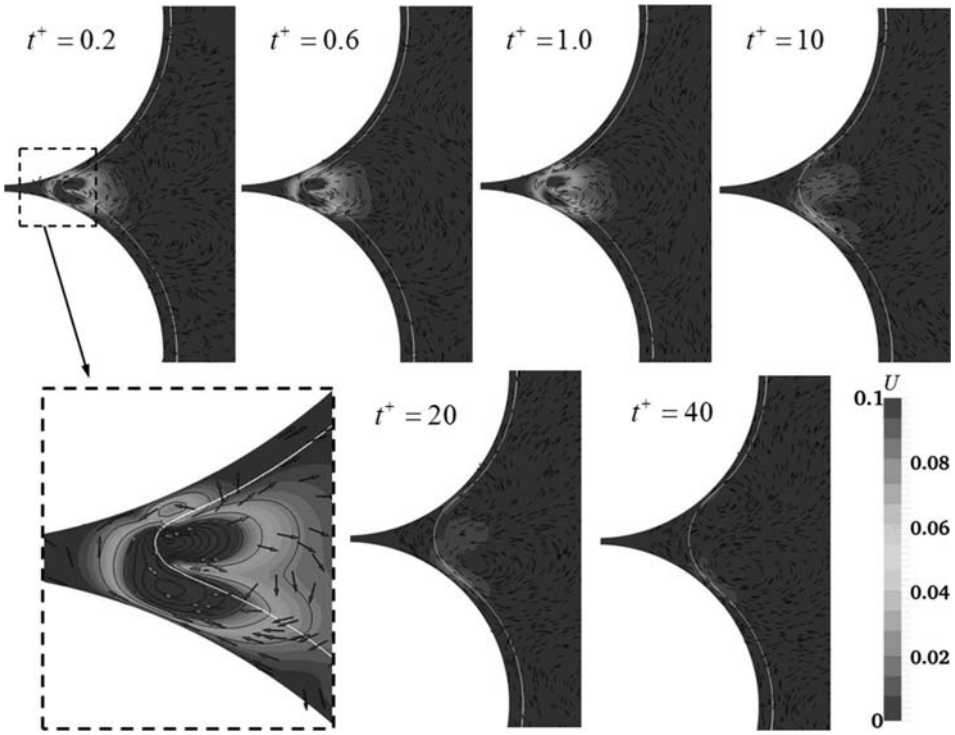

Figure 2. Typical velocity field for fluids flow over two fully coated particles using DNS.

[Color figure can be viewed in the online issue, which is available at wileyonlinelibrary.com.]

will overlap in physical reality, we define stage I to end after a (viscous) reference time scale of t_{ref}, that is, a dimensionless time of $t^+ = 1$. As shown next, we employ two different submodels to predict the liquid bridge volume in these two stages. By employing an overall mass balance it is then straight forward to predict the liquid residing on the contacting particles.

For the initial stage we simply aim on correlating the bridge volume after $t^+ = 1$ with the most important process parameters. Specifically, we simply choose the key geometrical parameters, which are (1) the initial film height h_0, as well as (2) the half separation distance S.

The next section of the article details on a postulated model to predict the time evolution of liquid bridge volume in stage II. Specifically, we use a phenomenological closure for the flow rate between the film and bridge compartment. We assume the flow rate to be proportional to the difference of the mobile fraction of the liquid on the particle and half of the bridge volume. To compute the mobile fraction of the liquid present on the particle, we use a single parameter which is called the mobility parameter $\phi_{m,i}$. This parameter is simply the ratio of the mobile liquid (i.e., the portion of liquid which flows into liquid bridge region) on a particle divided by the total liquid content on particle i. We will see in the "Results" section that the mobility parameter itself is a function of the initial film height and the particle separation, but is invariant in time. For now, we simply use $\phi_{m,i}$ as a parameter that is constant during the filling process. Using a dimensionless filling rate parameter a_i (which one can assume to be specific for each particle i) and the reference time scale t_{ref}, we finally arrive at the following differential equations for predicting the liquid content $L_{p,i}$ on each particle i:

$$\frac{dL_{p,i}}{dt} = \frac{-a_i}{t_{ref}}\left(L_{p,i}\phi_{m,i} - \frac{V_b}{2}\right) \tag{6}$$

This closure is linear in the unknown variables. Hence, an analytical solution for the liquid bridge volume and the liquid content remaining on the particles can be obtained. A simple mass balance yields the governing equation for the volume $V_{b,j}$ of bridge j:

$$\frac{dV_{b,j}}{dt} = -\sum_{i \in l_j} \frac{dL_{p,i}}{dt} \tag{7}$$

Here l_j is the list of particle indices that is in contact with bridge j. We now rewrite these equations in dimensionless variables, and apply them to a two-particle system. Together with appropriate initial conditions, as well as the assumption that a_i is a constant for a pair of particles sharing the same bridge, we arrive at the following analytical solution:

$$V_b^+ = V_{b,0}^+ + C_1 \frac{\frac{2r_1}{a_i} + 2\phi_{m1}}{r_1}\left(e^{r_1 t^+} - 1\right) + C_2 \frac{\frac{2r_2}{a_i} + 2\phi_{m1}}{r_2}\left(e^{r_2 t^+} - 1\right) \tag{8}$$

Table 1. Simulation Parameters and Numerical Schemes Used in the VoF Simulations

Parameter	Value	Comment
Δt^+	5×10^{-3}	Dimensionless time step
Δh	0.05–0.33	Dimensionless mesh resolution
Time derivative scheme	Backward	Second order, implicit
Laplacian scheme	Gauss linear corrected	Unbounded, second order, conservative
Convection scheme (for U)	Gauss linear	Unbounded, second order
Convection scheme (for α)	Gauss vanLeer	van Leer limiter

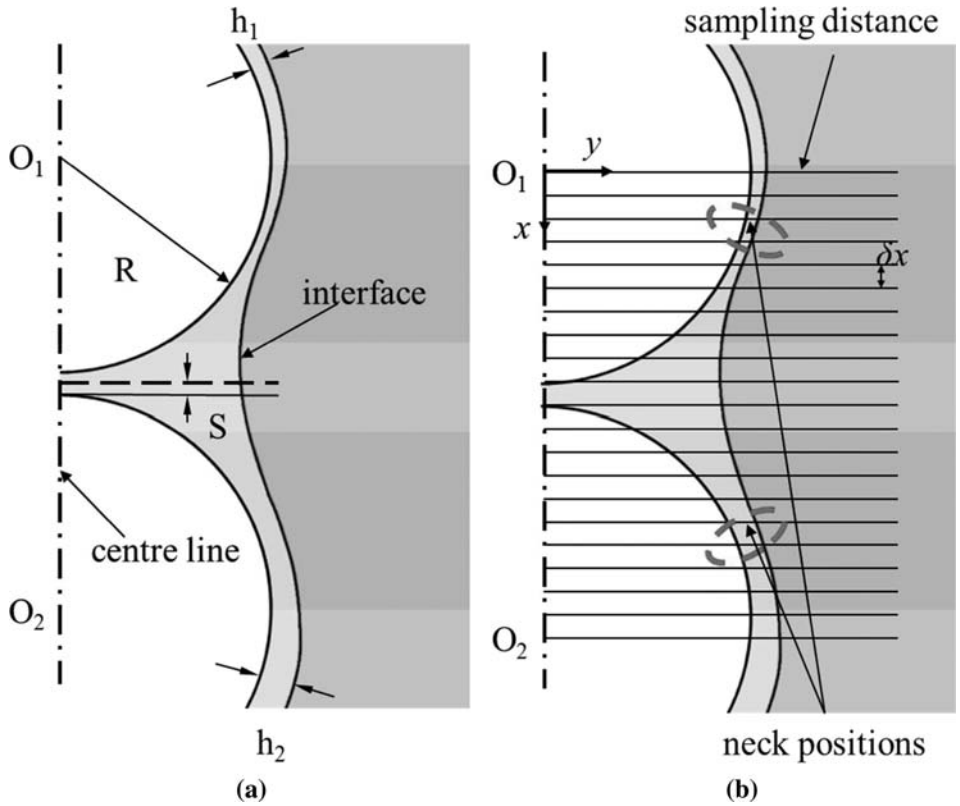

Figure 3. Sketch of (a) the gas–liquid interface between two particles, as well as (b) the sampling procedure used to detect the neck position.

[Color figure can be viewed in the online issue, which is available at wileyonlinelibrary.com.]

$$L_{p1}^{+}=L_{p1,0}^{+}+\frac{C_1}{r_1}\left(e^{r_1 t^{+}}-1\right)+\frac{C_2}{r_2}\left(e^{r_2 t^{+}}-1\right) \tag{9}$$

$$L_{p2}^{+}=L_{p2,0}^{+}-C_1\frac{\frac{2r_1}{a_i}+2\phi_{m1}+1}{r_1}\left(e^{r_1 t^{+}}-1\right) -C_2\frac{\frac{2r_2}{a_i}+2\phi_{m1}+1}{r_2}\left(e^{r_2 t^{+}}-1\right) \tag{10}$$

where r_1, r_2, C_1, and C_2 are dimensionless coefficients that are detailed in Appendix A. Using this solution it is now straight forward to calibrate the model parameters (i.e., a_i and $\phi_{m,i}$) with the results of our DNS (i.e., the time evolution of L_p and V_b).

Geometrical Bridge Volume

In order to close the proposed model (see "Results" section), it is useful to define a reference bridge volume based on geometrical arguments. For such a geometrical bridge volume we have considered two types which are illustrated in Figure 4. Our goal is to study liquid bridge formation between particles having initially a different liquid content. Thus, it is useful to define a bridge volume based on the average (i.e., arithmetic mean) film height h_0 (see the definition in previous section "VoF Simulation Approach"). The expressions for the geometrical bridge volume detailed below need to be understood as the typical volume of a liquid bridge when making certain assumptions about its shape.

Type I

Type I (Figure 4a) is a simple definition based on the assumption that the initial bridge volume is that in the cap-shaped region of the particle. This definition is similar to the idea of Shi and McCarthy[46], which assumed that a fixed fraction of the liquid present on the particle forms the bridge. This previous definition of Shi and McCarthy would predict a linear relationship between the bridge volume and the liquid film thickness (and, to a first approximation, also with the liquid content on each particle's surface). However, we argue that this previous definition is unrealistic. The reason for this is that the lateral extent (i.e., the length b) of the cap-shaped region defined by the gas–liquid interface and the symmetry plane between contacting particles is clearly a function of the film thickness (see Figure 4, left panel). Hence, for the present work we assume that the geometrical bridge volume of "type I" is a nonlinear function of the liquid film thickness. Specifically, we assume that the bridge volume is equal to the red-shaded cap-shaped region in Figure 4 (left panel). For this situation the liquid bridge volume can be calculated analytically:

$$V_{b,g,I}=2h_0 b^2\pi, \tag{11}$$

with

$$\frac{b}{R}=\left(1+h_0{}^{+}\right)\cos^{-1}\left(1/\left(1+h_0{}^{+}\right)\right) \tag{12}$$

Type II

Type II considers another shape of the liquid bridge, which is shown in Figure 4b. Here, we take the separation distance of the particle into account, implying that the type II geometrical bridge volume is more realistic for large separations. Specifically, we assume that the liquid in the overlapping regions (given by the assumed spherical shape of the liquid films on

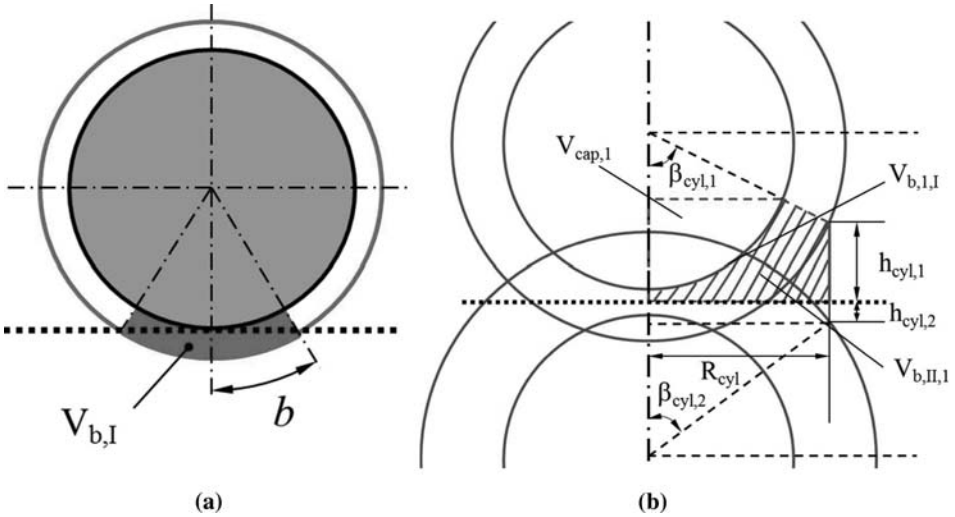

Figure 4. Geometrical bridge volume: (a) type I (the dashed line indicates the symmetry plane of two contacting particles), (b) type II.

[Color figure can be viewed in the online issue, which is available at wileyonlinelibrary.com.]

the particle) must be laterally displaced when the particles approach each other. This liquid is assumed to flow into a ring-shaped region. One can then compute the liquid bridge volume from the red shaded area (see Figure 4, right panel). Specifically, the volume of the type II bridge geometry can be calculated as follows:

$$V_{b,g,II} = V_{b,i,I} - V_{\text{cap}} \tag{13}$$

The evaluation of the above equation involves lengthy expressions, and is detailed in Appendix B. Unfortunately, this evaluation also requires an iterative procedure, making it less attractive for direct evaluation during large-scale DEM-based simulation.

We next compare these two types of models for the geometrical bridge volume for two situations: in situation A we increase the liquid content (i.e., the initial film heights), but assume contacting particles (i.e., zero separation between particles). Results for this situation are shown in Figure 5, which shows the dimensionless bridge volume as a function of the L_{p0}^{+}, where L_{p0}^{+} is dimensionless form of average amount of initial liquid content of the two particles and defined by $L_{p0}^{+} = \frac{4}{3}\pi\left((R+h_0)^3 - R^3\right)/R^3 = \frac{4}{3}\pi\left(\left(1+h_0^{+}\right)^3 - 1\right)$. We observe that for both types of definitions the bridge volume increase with the liquid content nonlinearly. Note, that in the definition of Shi and McCarthy[46] the bridge volume increases linearly. Furthermore, we see that the two curves for type I and type II nearly overlap, and that type II predictions are slightly larger than that of type I. Thus, the two curves agree well with each other for thin initial films, while they do not agree with each other for thicker films. Since the definition of the type II model at zero separation is close to that of type I, this is expected and explained as follows: the type II model takes into account that the laterally displaced liquid forms a bridge with a certain height $h_{\text{cyl},1}$ and $h_{\text{cyl},2}$ (see Figure 4, right panel). Consequently, a certain amount of the liquid on the particle (in addition to that accounted for in the type I model) is considered to be in the bridge. Thus, when using the type II definition, the (geometrical) bridge volume is somewhat larger compared to that predicted by type I. In summary, we see that the type I approximation is appropriate for thin films and at zero separation, while type II should be considered for all other situations.

Situation B is now investigated to demonstrate the effect of the particle–particle separation distance on the predicted (geometrical) bridge volume. Specifically, a certain (constant) initial film height was assumed for both types of models, and the separation between particles was varied. Results are illustrated in Figure 6. One can observe that the prediction of the type I model is not affected by the separation distance. However, for the type II model, the geometrical bridge volume remarkably decreases when the separation distance increases. Also, the type II model predicts a somewhat larger bridge volume (compared to type I) at zero separation as it should be. In summary, the type II model is more realistic, and we will demonstrate in following that our results (based on DNS) are very close to the predictions of this model.

Figure 7 further illustrates how the separation distance affects the prediction of the (geometrical) bridge volume when using the type II model. As can be seen from Figure 7 the

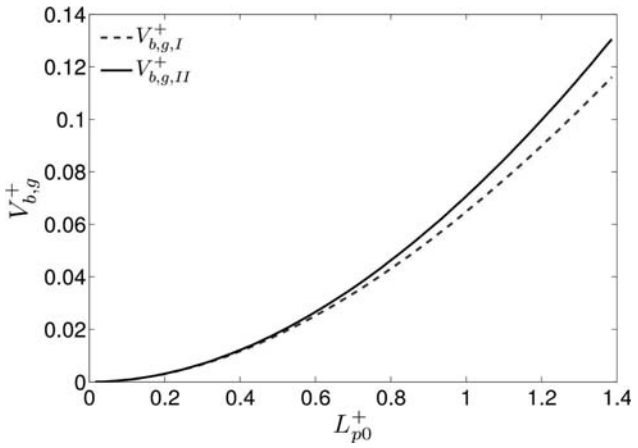

Figure 5. Comparison of the type I and type II model for computing the geometrical bridge volume in situation A: increasing liquid content on the particles at $S^{+} = 0$.

[Color figure can be viewed in the online issue, which is available at wileyonlinelibrary.com.]

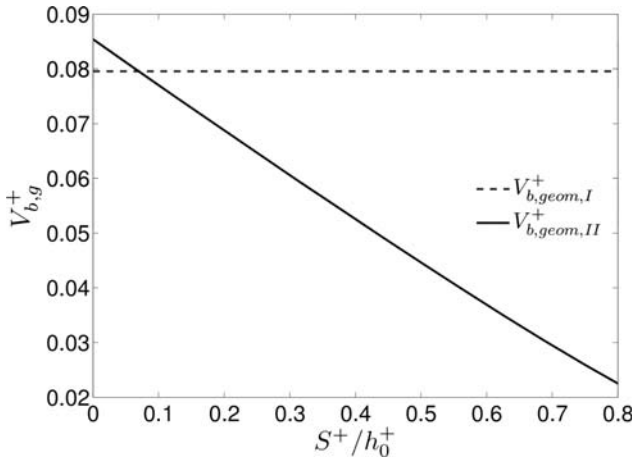

Figure 6. Comparison of the type I and type II model for computing the geometrical bridge volume in situation B: fixed initial film height $h_0^+ = 0.08$ and variation of the separation distance.

[Color figure can be viewed in the online issue, which is available at wileyonlinelibrary.com.]

bridge volume increases monotonically, but nonlinearly, with increasing (initial) liquid content for every choice of separation distance. In the situation of zero separation the largest bridge volume is predicted. Also, it can be observed that the bridge volume decreases almost linearly with increasing separation distance, finally approaching zero for $S^+/h_0^+ = 1$ as it should be. The physical interpretation of this fact is that for the situation in which the separation equals the initial film thickness, the overlapping region of thin films between two particles vanishes. Thus, the geometrical bridge volume becomes zero. In summary, the type II model shows the correct behaviour for a variety of limiting cases. Hence we argue that it is physically more relevant compared to previous work.

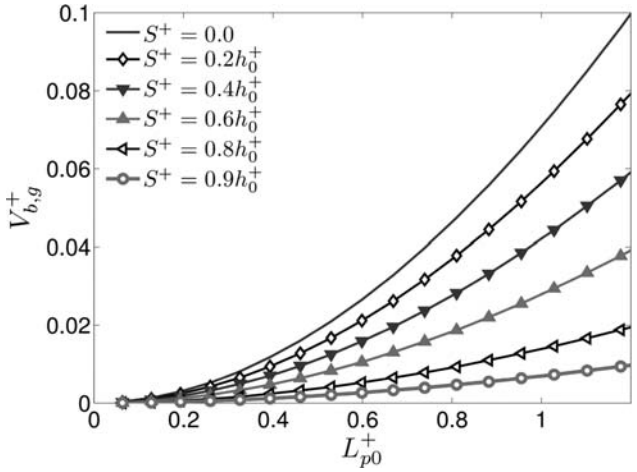

Figure 7. Effect of the separation distance on the bridge volume as a function of the initial liquid content (type II model).

[Color figure can be viewed in the online issue, which is available at wileyonlinelibrary.com.]

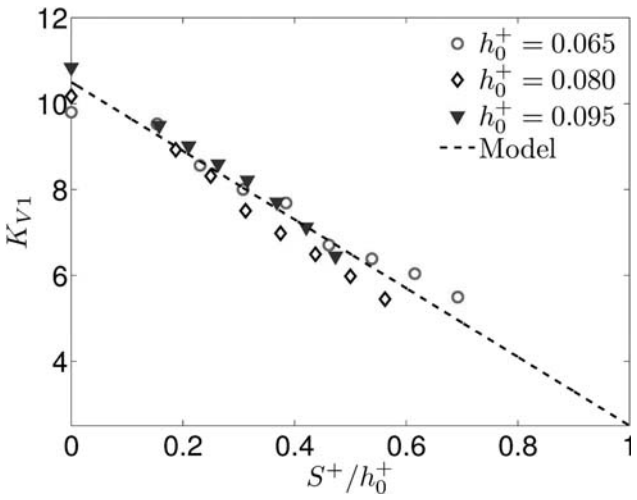

Figure 8. Normalized initial bridge model K_{V1} vs. normalized separation distance.

[Color figure can be viewed in the online issue, which is available at wileyonlinelibrary.com.]

Results

Early stage model (stage I)

The initial bridge forms very quickly, and the inertia of the fluid may play a certain role. Inertia is difficult to model due its inherent nonlinearity. We hence define a fixed initial bridge volume for "early times." Specifically, we have chosen the early stage to end after one reference viscous time scale, that is, at $t^+ = 1$.

We now attempt to model the initial bridge volume by defining the variable K_{V1}, which is the ratio of the simulated (total) initial bridge volume ($V^+_{b,0}$ is the liquid bridge volume at $t^+ = 1$) and the average initial film height h_0^+ to the power of some exponent n:

$$K_{V1} = \frac{V^+_{b,0}}{\left(h_0^+\right)^n} \tag{14}$$

This definition is based on the simple idea that the initial bridge volume is only a function of the (initial) film height, similar to the idea we used to define the geometrical bridge volume of type I. We see from Figure 8 that when choosing $n = 1.5$ we can collapse our DNS results for a variety of film thicknesses with the expression:

$$K_{V1} = -8.0\left(\frac{S^+}{h_0^+}\right) + 10.5 \tag{15}$$

Thus, we see that we can obtain a reasonable collapse of our data on a straight line for this choice of n and for $S^+/h_0^+ < 0.7$. We also note that (1) the normalized bridge volume linearly decreases with increasing separation distance, and (2) that the bridge volume is a super-linear function of the film height. The former fact is in agreement with the type II geometrical bridge volume (refer to "Geometrical Bridge Volume" section). The latter again stresses the fact that the assumption of Shi and McCarthy[46] that liquid is "harvest" from a fixed (area) fraction of the particle surface is not supported by our results. A model based on "harvesting" from a fixed (area) fraction of the particle surface would result in a linear increase of the bridge volume with film height, that is, $n = 1$. Clearly, this is not supported by our DNS data.

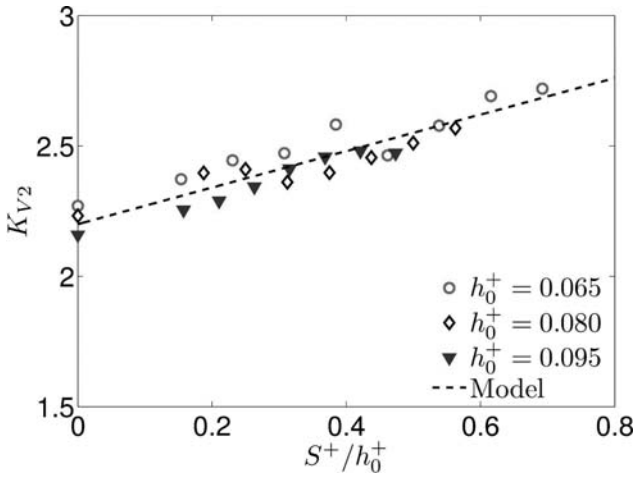

Figure 9. Initial bridge model, K_{V2} vs. normalized separation distance.

[Color figure can be viewed in the online issue, which is available at wileyonlinelibrary.com.]

In summary, our model for K_{V1} could already be used to compute $V_{b,0}^+$ for a collision involving two wet particles using Eq. 15. However, we next aim at using the geometrical bridge volume of type II to normalize the calculated initial bridge volume. We do this since this model accounts for the effect of the separation distance on the bridge volume, and we expect that a normalization with this geometrical bridge volume yields a variable that is independent of S^+.

Specifically, we define the variable K_{V2} as the ratio of the measured initial bridge, the geometrical bridge volume calculated using the type II model (refer to "Type II" section), and a function of h_0^+:

$$K_{V2} = \frac{V_{b,0}^+}{V_{b,g,II}^+ \left(h_0^+\right)^n} \tag{16}$$

Again, n is a parameter that is used as an exponent of the initial film height, and helps to collapse all data into a single curve. We expect that n is close to zero, that is, that the geometrical bridge volume based on the type II model is sufficient to account for any effects due to the film height. The results of our analysis are displayed in Figure 9, which illustrates that the variable K_{V2} is independent of the average film height, when choosing $n = 0.2$. For the K_{V2} model, we also suggest a linear relationship between the normalized liquid bridge volume and the separation distance:

$$K_{V2} = 0.7\left(\frac{S^+}{h_0^+}\right) + 2.2 \tag{17}$$

In addition we note that assuming $n = 0$, that is, using a normalization purely based on the geometrical bridge volume, would be also a good approximation (data not shown). Interestingly, we find that $K_{V2}\left(h_0^+\right)^n \approx 1.3$ for zero separation, indicating that the geometrical bridge volume of type II is indeed a good approximation of the initial bridge volume. Also, we find that K_{V2} increases with increasing separation, indicating that the geometrical bridge volume of type II overcompensates the decrease of the bridge volume. Thus, our DNS data suggest that the bridge volume is systematically larger for $S^+ > 0$ than that based on geometrical arguments. The exact reason for this is could not be isolated. However, it is clear that in the DNS the deformation of the gas–liquid interface is also taken into account. We speculate that this deformation leads to an additional lateral shift of the neck position (in addition to the shift caused by to the displaced fluid), which is more pronounced for larger separations.

In summary, the model for K_{V2} presented above, together with its definition, and the geometrical bridge volume (type II) can be used to compute the bridge volume at $t^+ = 1$. We next focus on the calibration of the parameters in the proposed bridge viscous filling model (see section "Proposed Model for Liquid Bridge Filling"), that can be used to predict the time evolution of the liquid bridge after this point in time.

Viscous filling stage model (stage II)

We start with looking at the time evolution of bridge volume and liquid present on the particle for the situation of zero separation start by taking one case for example (see Figure 10). We obtain the following parameter set $\phi_{m1} = 0.49$, $\phi_{m2} = 0.38$, and find that mobility parameter of particle 1 is somewhat larger than that of particle 2 (particle 1 initialized with less liquid content than particle 2). Furthermore, we find that the dimensionless filing rate coefficient a_i (i.e., the inverse of a dimensionless filling time scale) is approximately 0.025. This value fits all our data reasonably well, and hence we accept a_i to be a universal constant from now on.

Results in Figure 11 are also obtained for the zero separation case, however, for a different combination of film thicknesses. The mobility parameters for this case are $\phi_{m1} = 0.45$ and $\phi_{m2} = 0.43$, respectively. By comparing Figures 10 and 11, we observe that the trend of liquid transport between two particles are similar, and the model approximates the filling process reasonably well. As expected, the case with the larger (average) initial film height yields a larger liquid bridge volume.

Further testing of our model for other combinations of thickness reveals that our model is indeed able to describe the filling process well. As we can see from Figure 12, larger film height always leads to larger bridge volume, which is obvious. We also can see that the filling process levels off after about 50 dimensionless time units. This is also suggested by the inverse of the constant a_i, which has been fixed before.

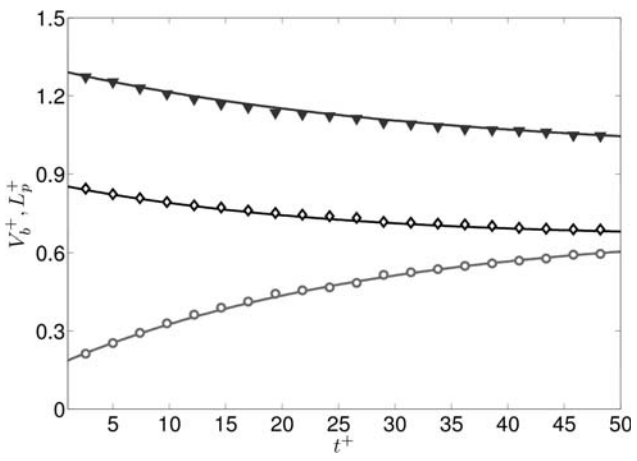

Figure 10. Fitted model (lines) vs. DNS data (symbols) over time for $S^+ = 0$, $h_1^+ = 0.07$, and $h_2^+ = 0.1$.

Red circles: liquid bridge volume (V_b^+); Black diamonds: liquid content on particle 1 (L_{P1}^+); Blue triangles: liquid content on particle 2 (L_{P2}^+). [Color figure can be viewed in the online issue, which is available at wileyonlinelibrary.com.]

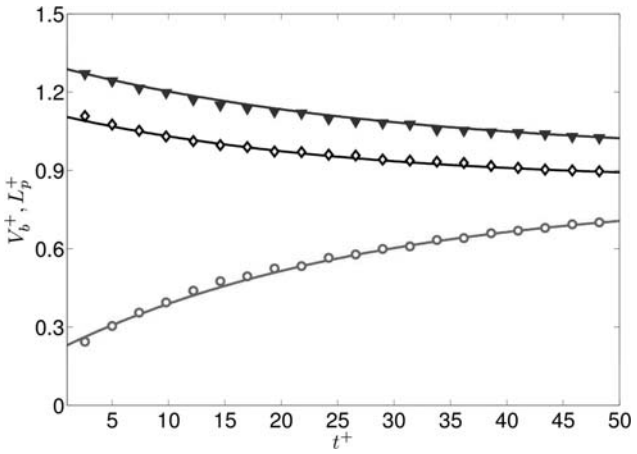

Figure 11. Fitted model (lines) vs. DNS data (symbols) over time for $S^+ = 0$, $h_1^+ = 0.09$ and $h_2^+ = 0.1$.

Red circles: liquid bridge volume (V_b^+); Black diamonds: liquid content on particle 1 (L_{P1}^+); Blue triangles: liquid content on particle 2 (L_{P2}^+). [Color figure can be viewed in the online issue, which is available at wileyonlinelibrary.com.]

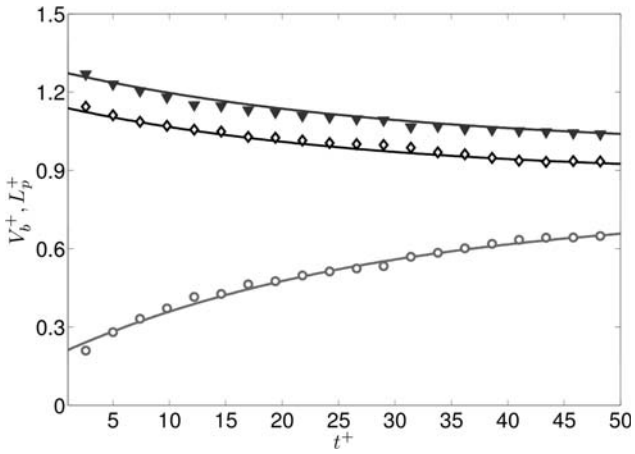

Figure 13. Fitted model (lines) vs. DNS data (symbols) over time for $S^+ = 0.045$, $h_1^+ = 0.09$ and $h_2^+ = 0.1$.

Red circles: liquid bridge volume (V_b^+); Black diamonds: liquid content on particle 1 (L_{P1}^+); Blue triangles: liquid content on particle 2 (L_{P2}^+). [Color figure can be viewed in the online issue, which is available at wileyonlinelibrary.com.]

However, the filling process has not completely stopped at $t^+ = 50$. Indeed, we find that when running the simulation for a longer duration the filling process will end at some point due to the rupture of the film on one of the two particle surfaces. We will discuss this peculiar behavior later (see section "Film Rupture and Grid Refinement").

Considering now separations larger than zero, we again see that the model is able to approximate the DNS data well (see Figure 13, for $S^+ = 0.045$, $h_1^+ = 0.09$, and $h_2^+ = 0.1$). However, we find that the parameters ϕ_{m1} and ϕ_{m2} change. Specifically, the value of the mobility parameters is now $\phi_{m1} = 0.42$ and $\phi_{m2} = 0.39$, respectively. Thus, the mobility of the liquid on the particles becomes smaller for $S^+ > 0$ compared to the case with $S^+ = 0$. Our interpretation of this fact is that less liquid is mobile to flow into the bridge when the particles have a certain separation. Again, we can see from Figure 14 that larger initial film height causes larger liquid bridge volume, as expected.

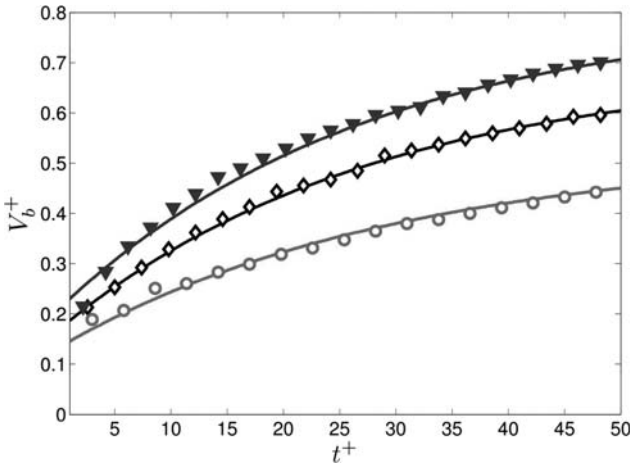

Figure 12. Liquid bridge volume over time: fitted model (lines) vs. DNS data (symbols), $S^+ = 0$.

Red circles: $h_0^+ = 0.075$; Black diamonds: $h_0^+ = 0.085$; Blue triangles: $h_0^+ = 0.095$. [Color figure can be viewed in the online issue, which is available at wileyonlinelibrary.com.]

We now aim on demonstrating that our model is able to represent data for a variety of dimensionless initial film heights. Since the key parameter that is influenced by the film height is the mobility (i.e., $\phi_{m,i}$), we have collected these parameters for a large set of separation distances and dimensionless initial film heights. We now make an attempt of modeling $\phi_{m,i}$ by first computing an average mobility ϕ_m (see Eq. 18), that is simply defined as the arithmetic mean of the motilities of the particles in contact. We now look at the trends of this average parameter as a function of the initial average film height. As we can see from Figure 15, ϕ_m changes linearly with the average initial film height for zero separation. Specifically, we obtain the following relationship for ϕ_m:

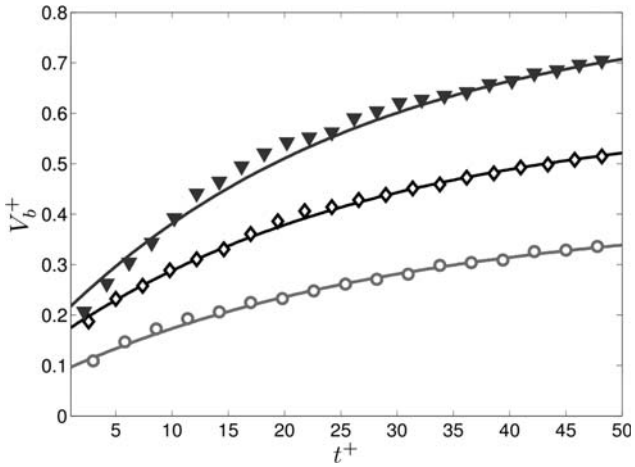

Figure 14. Combined effect of film height and separation distance: liquid bridge volume over time: fitted model (line) vs. DNS data (symbols).

Red circles: $S^+ = 0.045$ and $h_0^+ = 0.065$; Black diamonds: $S^+ = 0.025$ and $h_0^+ = 0.08$; Blue triangles: $S^+ = 0.035$ and $h_0^+ = 0.095$. [Color figure can be viewed in the online issue, which is available at wileyonlinelibrary.com.]

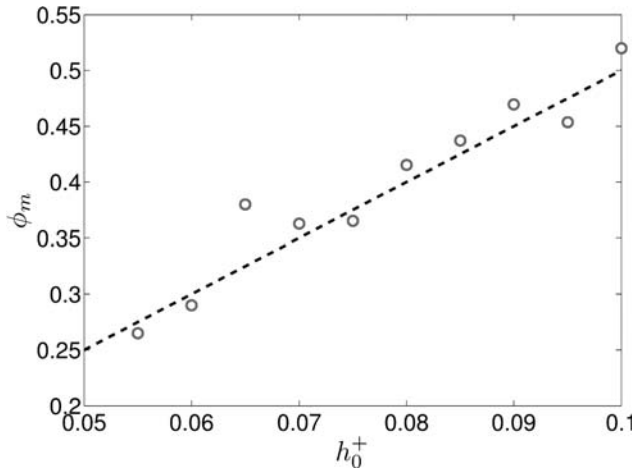

Figure 15. ϕ_m as a function of h_0^+ for a separation of $S^+ = 0$.

[Color figure can be viewed in the online issue, which is available at wileyonlinelibrary.com.]

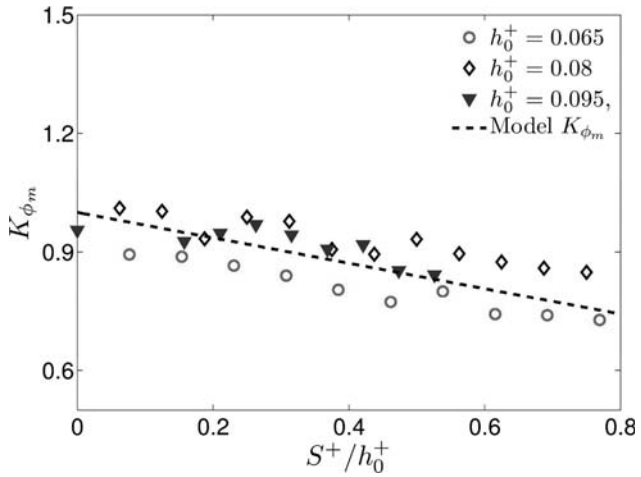

Figure 17. K_{ϕ_m} as a function of the normalized separation distance for contacting and non-contacting particles.

[Color figure can be viewed in the online issue, which is available at wileyonlinelibrary.com.]

$$\phi_m = \frac{\phi_{m1} + \phi_{m2}}{2} \tag{18}$$

$$\phi_m = 5h_0^+ \tag{19}$$

For the difference in the mobilities, denoted as $\Delta\phi_m = |\phi_{m1} - \phi_{m2}|$ and illustrated in Figure 16, we find the following approximation:

$$\Delta\phi_m = 2.9\Delta h_0^+ \tag{20}$$

Next, we aim at correlating ϕ_m with the separation distance. Specifically, we consider data sets for variations in the initial film height and separation distance shown in Figure 17. Again, we can collapse all data for different initial film heights when normalizing it with some function of the initial film height. Specifically, we define the variable $K_{\phi m}$ to be

$$K_{\phi_m} = \frac{\phi_m}{5h_0^+} \tag{21}$$

Based on the data shown in Figure 17, we find the following relationship for $K_{\phi m}$:

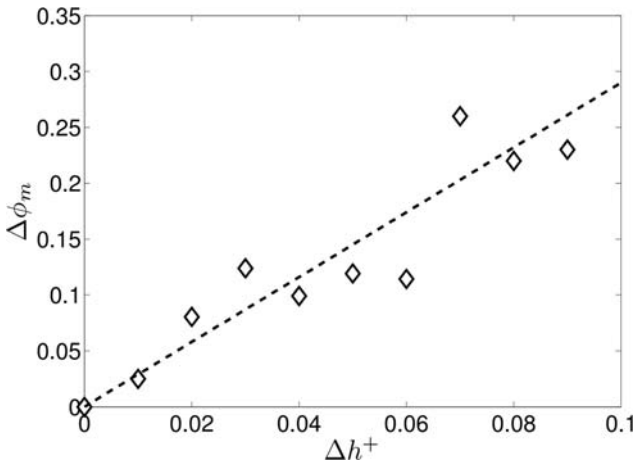

Figure 16. $\Delta\phi_m$as a function of the dimensionless difference of the film heights.

$$K_{\phi_m} = 1 - 0.32\left(\frac{S^+}{h_0^+}\right) \tag{22}$$

The meaning of these relationships is that the average mobility of the liquid on the particle surfaces systematically decreases with increasing separation distance. The physical interpretation of this fact is that smaller bridges (implied by larger separation distances and constant overall liquid content) simply allow proportionally less liquid to flow from the particle surface into the bridge. In contrast, at small separation distances, and hence larger bridges, a larger fraction of the particle's surface area is connected to the bridge, and hence the mobility parameter is large.

Film rupture and grid refinement

We also show some interesting findings which we observe for very long simulation times and thin films: as can be seen in Figure 18 the film ruptures at the neck position for sufficiently long time. Specifically, we observe that for thin films the film ruptures on the particle with initially less liquid (i.e., particle 1). This means that the bridge filling process stops after a certain time, which is also the case for the proposed model. Unfortunately, we cannot accurately predict the rupturing process, simply because the film at the rupturing point must become thinner than the (finite) grid resolution. It is therefore essential how the grid resolution affects the film rupturing event. This is discussed next.

We start our investigation of the effect of grid refinement by defining a dimensionless grid size Δh. Specifically, we choose $\Delta h = \Delta x/h_1$, where Δx is the mesh size and h_1 is the initial film height of the particle with the lower amount of liquid on its surface. As can be seen from Figure 19, the grid refinement affects the filling process only negligibly, with the largest deviations observed for long times, that is, $t^+ > 100$. As can be seen in the Figure for the case of a grid size of $\Delta h = 0.17$ (blue circles) film rupture is observed at $t^+ = 175$. However, in case of a larger grid resolution, that is, $\Delta h = 0.12$ (black diamonds), we do not observe film rupture and the filling process continues until the simulation was terminated. Therefore, grid refinement plays an important role for

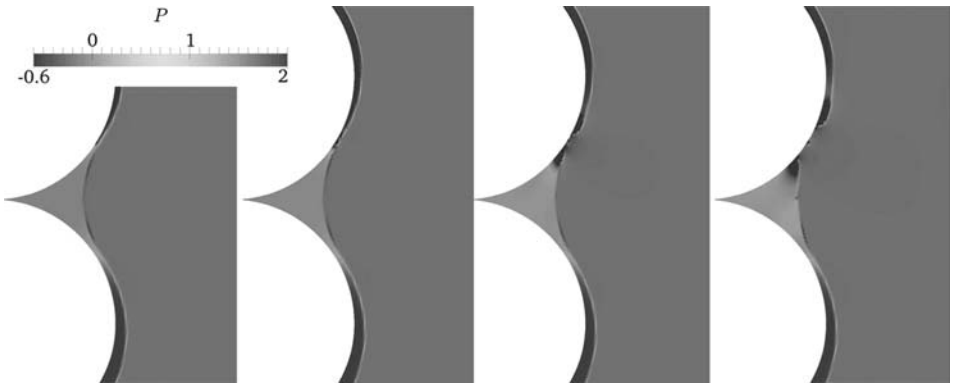

Figure 18. Pressure distribution before and after the film rupture moment $t^+ = 220$, $S^+ = 0$, $h_1^+ = 0.06$, $h_2^+ = 0.10$ (the rupture time scale is small, that is, below $t^+ < 1$).

[Color figure can be viewed in the online issue, which is available at wileyonlinelibrary.com.]

predicting the final rupturing process. Moreover, it can be observed that a finer mesh yields a rather smooth curve, in contrast to the results for the coarser grid in which the bridge volume appears to fluctuate. This is again caused by the more challenging detection of the neck position in the case of a (comparably) coarse grid.

We have observed in our simulations that the film rupturing phenomena occurs on particles with less liquid. The obvious reason for film rupturing in the simulation is inadequate resolution of the liquid film in the neck region. The thinning of the film there is caused by the pressure difference over the neck region, which drives the flow of liquid into the bridge: due to the complex shape of the gas–liquid interface in this region, the pressure changes in a nonlinear way in the neck region. The pressure distribution is such that more liquid exits the neck region than can flow from the film toward the neck. This leads to a thinning of the film, and once the film thickness is in the order of the grid resolution, it will rupture. We hence must limit the applicability of our model to situations well before the rupture event occurs in the simulation, that is, to $t^+ < 100$.

Reynolds number and density ratio effects

In order to further investigate the model's ability to reflect various real-world situations, we checked the effect of the Reynolds number on the filling process. Therefore, we have chosen a situation with rather thin films (i.e., $h_1^+ = 0.04$, $h_2^+ = 0.08$, $S^+ = 0.02$). We choose $Re = 1$, $Re = 100$, and $Re = 10{,}000$ for investigating Reynolds number effects.

As we can see from Figure 20, the points at which film rupture occurs are almost identical. Also, we observe that larger Reynolds number lead to an earlier film rupturing event (see Figure 21). However, the filling process of the bridge is not substantially affected by the Reynolds number. Hence, we draw the conclusion that the Reynolds number plays a negligible role for the bridge filling process, at least in the range of parameters we have investigated.

Finally, we have investigated the effect of the density ratio on the liquid bridge filling process (see our results in Figure 22 for the density ratios of $\rho = 10$, and $\rho = 1000$). The density ratio is a critical parameter for the numerical simulation, since simulations with a smaller density ratio are typically easier to conduct. As can be seen from Figure 22 the density ratio has little effect on the liquid bridge filling process as long as $\rho \geq 10$, and the rupturing event is delayed by about five dimensionless time units in the case of the low density ratio that has been investigated. Therefore, we can safely neglect effects due to the ambient gas density when considering bridge filling in gas–liquid-particle systems.

Initial bridge shape effects

In this section we summarize data on the effect of the initial shape of the liquid bridge on the bridge filling process. As shown in Figure 23, four types of initial bridge shapes have been investigated, that is, the standard cylinder (denoted as "cylinder"), no bridge ("none"), a too large cylinder ("large cylinder"), i.e., the radius is 20% larger than standard cylinder, and a smooth curve in the form of a circle ("circle"). The results are shown in Figure 24, and we observe that the initial liquid bridge shape has generally a small effect on the filling process, except for the situation "large cylinder". For this situation significantly more liquid is in the bridge, however, the qualitative behavior of the filling process is preserved. Hence, we conclude that as long as the bridge is initialized with a realistic shape (i.e., a cylinder containing the displaced fluid), the effect of the exact initial shape is in the order of 3.3% between "none" and "cylinder", and 3.9% between "circle" and "cylinder".

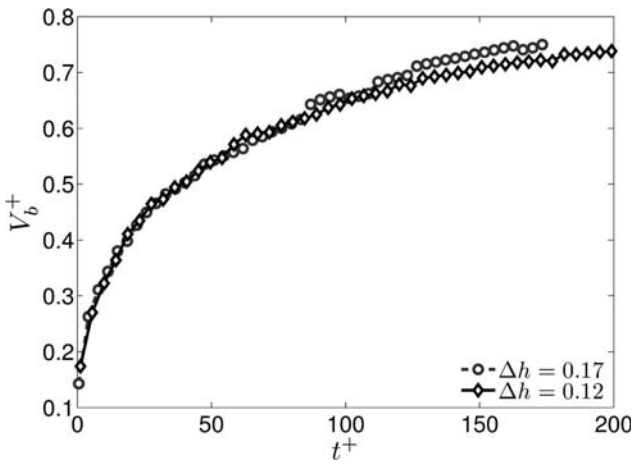

Figure 19. Grid refinement effects on the liquid bridge filling, $h_1^+ = 0.04$, $h_2^+ = 0.08$, $S^+ = 0.02$.

[Color figure can be viewed in the online issue, which is available at wileyonlinelibrary.com.]

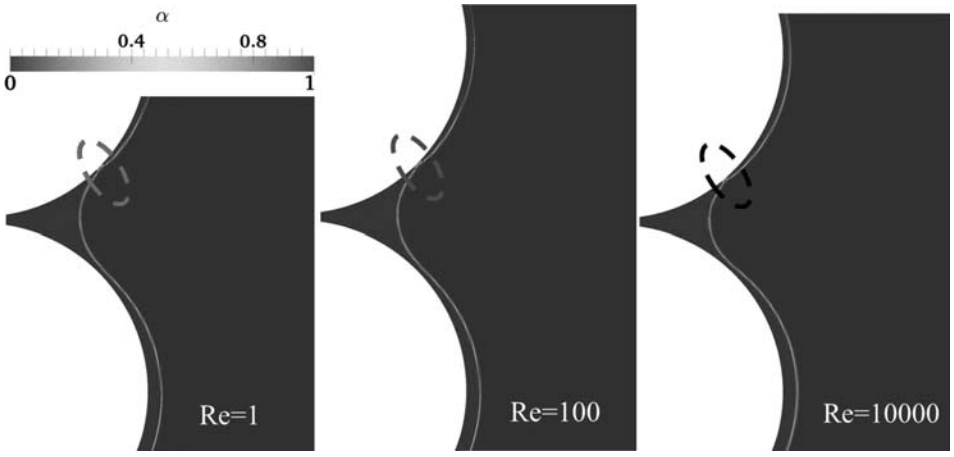

Figure 20. Liquid film distribution at the rupture moment, $h_1^+ = 0.04$, $h_2^+ = 0.08$, $S^+ = 0.02$.

[Color figure can be viewed in the online issue, which is available at wileyonlinelibrary.com.]

Discussion

In our study, we investigate the liquid bridge and drainage process of liquid adhering to two wet particles based on key dimensionless parameters. We provide a model for the prediction of dynamic liquid-bridge formation between two particles by assuming that the filling rate of the liquid bridge is not affected by the particles' relative motion. Thus, we assume a quasi-static situation in which particles do not move, but only liquid is mobile to flow into the bridge. We next perform a time scale analysis to probe situations for which such a quasi-static assumption is appropriate.

Particle interaction time scales

A key question that could not be answered in the current article is what happens in case the particles move relative to each other, and hence the above mentioned quasi-static assumption breaks down. In order to do so, we must identify the limits of the models proposed in the current work. Specifically, there are two criteria that need to be satisfied to accept the assumption of zero relative particle velocity:

1. The time scale for bridge formation must be smaller than a characteristic time scale (denoted as t_{acc}) for the particles to accelerate to a typical speed of liquid flow (i.e., $u_{ref} = \sigma/\mu_l$). Physically this means that the speed of the particle relative motion is smaller than the speed of liquid flow.

2. The time scale for bridge formation must be smaller than the time (denoted as t_{cross}) it takes for the particles to cross the film.

The acceleration time scale t_{acc} can be calculated from the force balance on a particle. Assuming that the liquid bridge only exhibits a cohesive force due to surface tension, the dimensional acceleration time scale (such that the particle have accelerated to the typical liquid flow speed u_{ref}) is $t_{acc} = R^2\rho_p/\mu_l$. The corresponding dimensionless acceleration time scale (with $t_{ref} = R\mu_l/\sigma$ being the reference time scale) is:

$$t_{acc}^+ = \frac{R\rho_p\sigma}{{\mu_l}^2} \tag{23}$$

The time for an approaching particle to cross the film, that is, t_{cross}, can be calculated from a typical particle–particle relative velocity u_{rel} and the film thickness, that is, $t_{cross} = h_0/u_{rel}$.

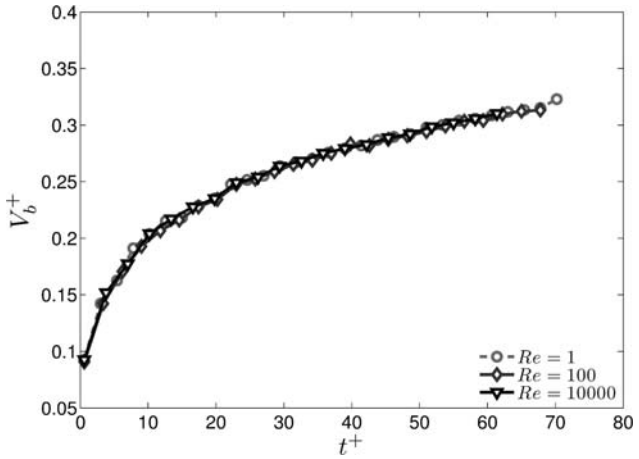

Figure 21. Reynolds number effect on liquid bridge filling, $h_1^+ = 0.04$, $h_2^+ = 0.08$, $S^+ = 0.02$.

[Color figure can be viewed in the online issue, which is available at wileyonlinelibrary.com.]

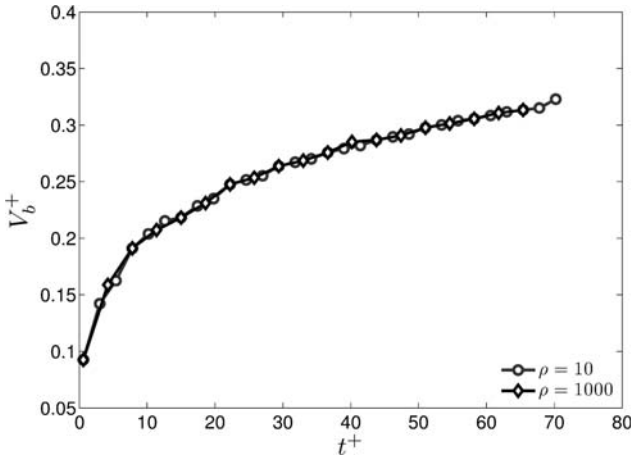

Figure 22. Density ratio effect on bridge volume filling, $h_1^+ = 0.04$, $h_2^+ = 0.08$, $S^+ = 0.02$.

[Color figure can be viewed in the online issue, which is available at wileyonlinelibrary.com.]

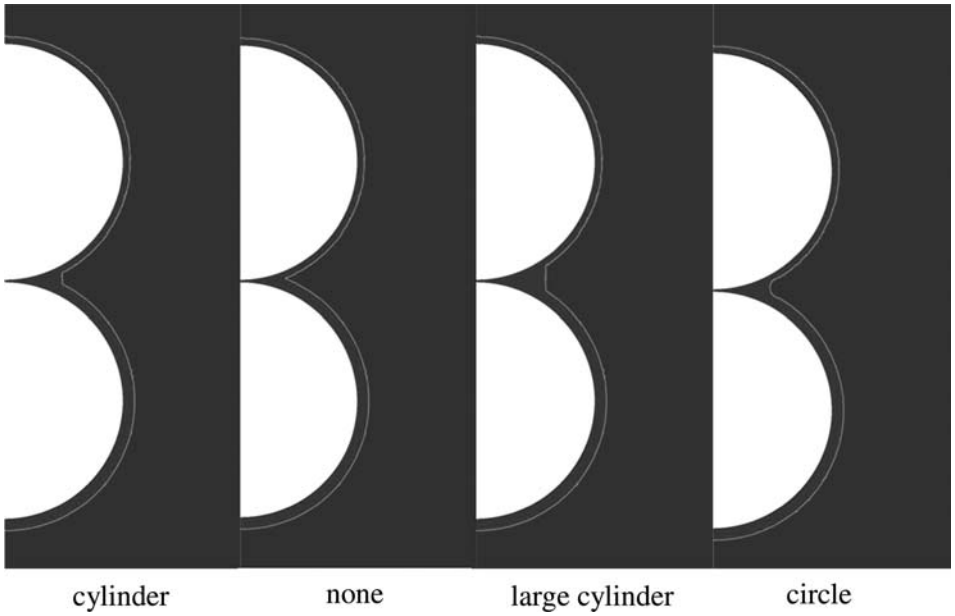

Figure 23. Different shapes of the initial liquid bridge ($h_1^+ = 0.06$, $h_2^+ = 0.10$, $S^+ = 0.01$).

[Color figure can be viewed in the online issue, which is available at wileyonlinelibrary.com.]

Using Stokes settling velocity as u_{rel}, one obtains for the dimensionless crossing time scale:

$$t^+_{\mathrm{cross}} = \frac{9h_0^+ \mu_g \sigma}{2R^2 \mu_l \left(\rho_p - \rho_g\right) g} \tag{24}$$

Here $h_0^+ = h_0/R$ is the dimensionless film-thickness, μ_g is the ambient gas viscosity, and ρ_p is the particle density. Note, that the alternative assumption of $u_{\mathrm{rel}} = u_{\mathrm{ref}} = \sigma/\mu$ would lead to $t^+_{\mathrm{cross},u_{\mathrm{ref}}} = h_0^+$. However, as explained above in the discussion of t_{acc}, it takes time to accelerate the particles to the capillary speed. Hence, the latter velocity scale is certainly of lower importance for typical applications that are characterized by a large particle Stokes number.

In case both dimensionless time scales are much larger than unity, the assumption of nonmoving particles in our simulations is acceptable. By assuming typical properties of various water–glycerine mixtures,[49] and using parameters typical for a T2 fluidized bed, we have summarized key dimensionless parameters in Table 2 and Figure 25. It can be seen that for most fluidized bed systems the assumption of zero relative particle velocity when modeling liquid transfer is justified. Tables 2 T3 and 3 list relevant system parameters for particulate systems involving pure water, as well as mixtures of glycerine and water (60 and 40%). In general, situations with highly viscous fluids (i.e., pure glycerine), appear to conflict with our quasi-static assumption. For these situations the relative velocity of the particles might influence the bridge filling process. However, for most systems involving typical liquids with a water-like viscosity (see Tables 2 and 3, as well as the illustration in Figure 25), we find that the assumption of zero relative particle velocity is adequate.

Viscous effects during particle approach

The acceleration time scale defined above is based on Newton's law of motion considering capillary forces only. Clearly, viscous forces will retard the particles' relative motion, and hence we expect that the typical particle interaction time is larger than t^+_{acc}. Next, we analyze such a situation by including lubrication effects due to the liquid between two approaching wet particles. For such a situation we have:

$$\vec{F}_{\mathrm{vis}} + \vec{F}_{\mathrm{cap}} = m\frac{d\vec{u}}{dt} \tag{25}$$

where $\vec{F}_{\mathrm{vis}}$ is the viscous force, $\vec{F}_{\mathrm{cap}}$ is the capillary force, and m is the mass of one particle. For small particles (i.e., in case the particle size is smaller than the capillary length), the gravitational forces can be neglected, and only capillary and viscous forces affect particle motion. Pitois et al.[14] and Darabi et al.[2] applied the lubrication approximation for liquid flow between the two particle surfaces, and arrived at the following expression for the viscous force:

$$\vec{F}_{\mathrm{vis}} = -\frac{3}{2}\pi\mu R^2 X_v^2 \frac{1}{S}\frac{dS}{dt}, \tag{26}$$

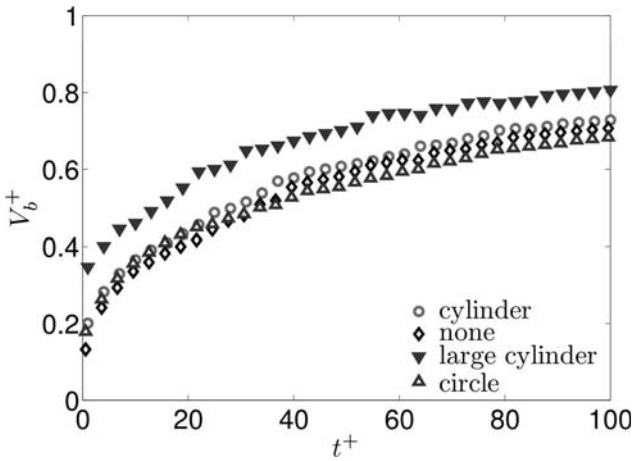

Figure 24. Effect of the initial bridge shape on the bridge filling process ($h_1^+ = 0.06$, $h_2^+ = 0.10$, $S^+ = 0.01$).

[Color figure can be viewed in the online issue, which is available at wileyonlinelibrary.com.]

Table 2. Summary of Parameters Relevant for Liquid Transfer in Typical Fluidized Beds (for t^+_{cross} Refer to Figure 25)

Glycerine/water	R [m]	ρ_p [kg·m^{-3}]	h_0^+	t_{ref} [s]	t^+_{acc}	Oh
Water	5e-6	1000	0.01	6.86e-8	363.5	0.052
Glycerine/water-60/40%	5e-6	1000	0.01	8.54e-7	2.54	0.58
Glycerine/water-79/21%	5e-6	1000	0.01	3.86e-6	0.13	2.53
Glycerine/water-90/10%	5e-6	1000	0.01	1.74e-5	6.55e-3	11.1
Pure glycerine	5e-6	1000	0.01	8.87e-5	2.52e-4	56.13
Water	5e-6	1000	0.1	6.86e-8	363.5	0.052
Glycerine/water-60/40%	5e-6	1000	0.1	8.54e-7	2.54	0.58
Glycerine/water-79/21%	5e-6	1000	0.1	3.86e-6	0.13	2.53
Glycerine/water-90/10%	5e-6	1000	0.1	1.74e-5	6.55e-3	11.1
Pure glycerine	5e-6	1000	0.1	8.87e-5	2.52e-4	56.13
Water	5e-3	1000	0.1	6.86e-5	3.64e5	1.66e-3
Glycerine/water-60/40%	5e-3	1000	0.1	8.54e-4	2.54e3	1.85e-2
Glycerine/water-79/21%	5e-3	1000	0.1	3.86e-3	130	0.08
Glycerine/water-90/10%	5e-3	1000	0.1	1.74e-2	6.55	0.35
Pure glycerine	5e-3	1000	1e-4	8.87e-2	0.25	1.77
Water	5e-6	5000	0.1	6.86e-8	1717	0.052
Glycerine/water-60/40%	5e-6	5000	0.1	8.54e-7	12.7	0.58
Glycerine/water-79/21%	5e-6	5000	0.1	3.86e-6	0.65	2.53
Glycerine/water-90/10%	5e-6	5000	0.1	1.74e-5	0.033	11.1
Pure glycerine	5e-6	5000	0.1	8.87e-5	1.25e-3	56.13

$$X_v = 1 - 1/\sqrt{1 + \frac{2V_b}{\pi R S^2}}. \tag{27}$$

where R is the particle radius, S is the half separation distance between the particle surfaces, and V_b is the liquid bridge volume. Pitois et al.[14] and Darabi et al.[2], also provided a model for the capillary force that accounts for the bridge volume effect. For fully wetted particles their capillary force model is:

$$\vec{F}_{cap} = 2\pi R \sigma X_v \tag{28}$$

Substituting the model for the viscous and capillary force into Eq. 25, and using typical initial conditions (i.e., an initial separation of 10% of the particle radius, and particles initially at rest), we obain the following differential equation:

$$\begin{cases} -\frac{3}{2}\pi\mu_l R^2 X_v^2 \frac{1}{S}\frac{dS}{dt} + 2\pi R\sigma X_v = m\frac{d^2S}{dt^2} \\ S(0) = 0.1R \ ; \qquad S'(0) = 0. \end{cases} \tag{29}$$

Integrating the above equation in time is straight forward (e.g., using Matlab®), and we have chosen two sets of parameters, that is, that of water and pure glycerine to illustrate the solution. Relevant properties for these liquids are listed in Table 4. The particle size is chosen to be 10 μm, the liquid bridge volume is chosen to be 20% of the particle volume, the Reynold number is defined by the capillary speed, the particle radius, and the fluid viscosity (i.e., $\mathrm{Re} = \sigma R \rho_l / \mu_l^2$). One can also define a capillary number Ca to quantify the ratio of viscous and capillary effects. This number is based on the Stokes setting velocity (as a proxy for the relevant particle–particle relative speed), the viscosity of the liquid, and the surface tension, that is, $Ca = \mu_l u_{rel}/\sigma = \left(2\,\mu_l R^2 \left(\rho_p - \rho_g\right) g\right) / \left(9\mu_g \sigma\right)$. In summary, we obtain for

- pure glycerine: $Re = 6.34 \times 10^{-4}$, $Ca = 0.975$, and for
- water: $Re = 730$, $Ca = 7.54 \times 10^{-4}$

Figure 26 illustrates the time evolution of the particle separation distance, as well as the acceleration time scale derived above. Figure 27 summarizes the corresponding relative velocity scaled with the reference velocity, that is, a typical speed of the adhering liquid when flowing into the bridge. We can observe from Figure 26 (dashed and continuous bold line) that the time until contact is larger than t^+_{acc} for the glycerine

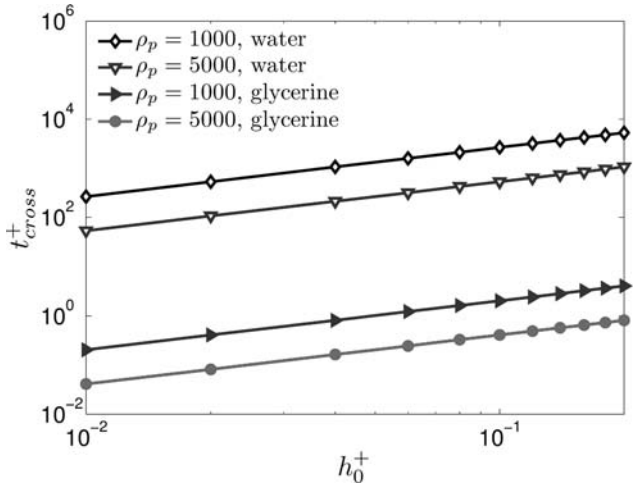

Figure 25. t^+_{cross} for water and pure glycerine in typical fluidized bed operations.

[Color figure can be viewed in the online issue, which is available at wileyonlinelibrary.com.]

Table 3. Effect of Selected Particle Parameters on Dimensionless Bridge Filling Parameters for Glycerine/Water-60/40% Mixtures

Cases	R [m]	ρ_p [kg·m^{-3}]	h_0^+	t_{ref} [s]	t^+_{acc}	t^+_{cross}	Oh
1	5e-6	1500	1e-2	8.54e-7	3.82	14.2	0.58
2	5e-6	1500	0.2	8.54e-7	3.82	284	0.58
3	1e-5	1500	0.1	1.71e-6	7.63	35.5	0.41
4	1e-5	2000	0.1	1.71e-6	10.18	26.6	0.41
5	1e-5	5000	0.1	1.71e-6	25.44	10.6	0.41

Table 4. Properties of Different Water-Glycerine Mixtures (Adapted from Eddi et al.[49])

Mixture	μ [Pa·s]	ρ [kg·m^{-3}]	σ [N/m]
Water	1×10^{-3}	1000	0.073
Glycerine/water-60/40%	0.0115	1153	0.0673
Glycerine/water-79/21%	0.05	1204	0.0647
Glycerine/water-90/10%	0.22	1238	0.0634
Pure glycerine	1.12	1262	0.0631

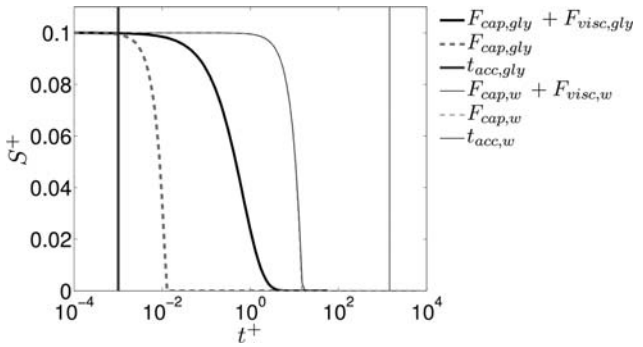

Figure 26. Time evolution of the half separation distance S^+ during the acceleration phase of two approaching particles ($\rho_p = 2000$ [μm], $d_p = 10$ [μm], $V_b^+ = 0.1$).

[Color figure can be viewed in the online issue, which is available at wileyonlinelibrary.com.]

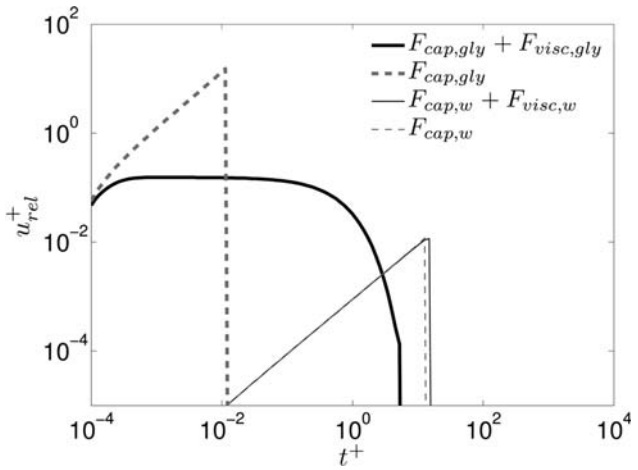

Figure 27. Time evolution of the relative particle velocity during the acceleration phase of two approaching particles (parameters are the same as in Figure 26).

[Color figure can be viewed in the online issue, which is available at wileyonlinelibrary.com.]

system. Thus, the particles accelerate, but only for the situation where viscous forces are neglected the particle accelerate beyond u_{ref} (see Figure 27). In contrast, in the system involving water the particles' relative speed never excees u_{ref}, and the impact speed is in the order of 0.01 u_{ref} (see thin dashed and continuous line in Figures 26 and 27). As expected, lubrication forces resist the particle's relative motion and delay the time until contact (see continuous lines in Figures 26 and 27). This effect is more pronounced for the viscous systems, while the effect in the system involving water is rather small. Clearly, in case one does not take into account the viscous term (see Eq. 26) for the glycerine system, the particles accelerate to an unphysically large relative velocity. In case we account for viscous forces, however, we expect typical particle relative speeds smaller than 0.1 u_{ref}, even for highly viscous systems (see Figure 27). These particle velocities are below the typical liquid speed for early times (i.e., $t^+ = 1$, see Figure 2). For longer times both the liquid and particle speed decreases rapidly, the particles' surfaces touch (at t^+ between 5 and 50 depending on the viscosity of the liquid, see Figure 27). Hence, bridge filling is also unaffected by particle motion for longer times, simply because the particles are already in contact. Based on the above consideration of particles accelerating from zero velocity, it appears that our assumption of a quasi-static liquid bridge formation is valid for a wide range of wet particulate systems.

Typical impact speeds in sedimenting suspensions

The typical relative particle velocity at impact is important for our analysis, since it affects the scale for film crossing. We have therefore performed simulations of a typical application we are interested in (i.e., wet granulation in a fluidized bed). Specifically, we considered a freely sedimenting suspension, and have recorded the speed and orientation of particle–particle collisions. The simulations followed the approach used by Radl and Sundaresan[50], with identical fluid and particle

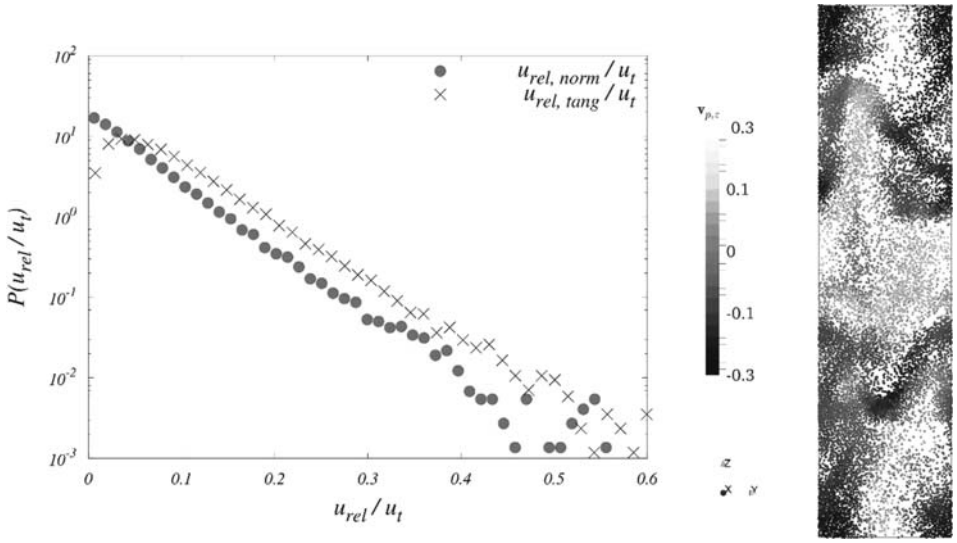

Figure 28. Distribution of particle collision velocities in the normal and tangential direction (left panel), as well as illustration of the vertical particle velocity distribution (right panel, $d_p = 150$ [μm], $\rho_p = 1500$ [kg/m^3], $\phi_p = 0.10$, particles sediment in air at ambient conditions).

[Color figure can be viewed in the online issue, which is available at wileyonlinelibrary.com.]

F28 properties. Our results are summarized in Figure 28, highlighting that collisions in typical applications we are interested in (i.e., fluidized beds) are mostly gentle: the typical impact speed is in the order of 10% of the particles' terminal settling velocity. Also, we observe from Figure 28 that particle collisions are primarily oblique, that is, the particles' relative speed in the tangential direction (at the contact point) is smaller than that in the normal direction. In Appendix C we summarize more data for sedimenting suspensions, which show a similar qualitative behavior and a moderate increase of the impact speed when decreasing the particle concentration. Clearly, our data supports our assumption of quasi-static bridge filling for a wide range of wet particulate systems with rather thick liquid films and a rather low liquid viscosity.

Of course, the relative speed of particles in a wet collision event is set by the process, and we have only considered a wet fluidized bed here. Clearly, it is necessary to check the appropriateness of our model for a specific application via a prior analysis of typical particle relative velocities.

Conclusions

A new model to predict dynamic liquid bridge formation between two wet particles has been presented in this article. This model is based on DNS data, which were obtained by extracting the interface position from VoF-based simulations of the bridge filling process. The liquid bridge volume was defined based on a characteristic neck position, and a DIM was employed to calculate the liquid bridge volume. This allowed us building a dynamic model for predicting the bridge volume, and the liquid remaining on the particle surfaces. Such a model might help to refine our picture of wet particle collisions that previously focused exclusively on predictions of the coefficient of restitution (Donahue et al.[24], Sutkar et al.[28]).

Our model differentiates between (1) a fast initial bridge formation stage where the dimensionless time is less than a reference time for capillary-driven viscous flow, and (2) a subsequent slower viscous filling stage where viscous effects are dominant. The initial stage model is based on a geometrical reference volume, and has been calibrated with DNS data at a dimensionless time of $t^+ = 1$. Our initial stage model can be used as a first estimate for the liquid bridge volume in short particle collisions, and is an extension of the model prosed by Shi and McCarthy[46]. The postulated model for the viscous filling stage model relies on a universal parameter a_i (i.e., a characteristic dimensionless filling time), as well as dimensionless liquid mobility parameters ϕ_{m1} and ϕ_{m2} of the contacting particles. A model equation for these mobility parameters has been proposed. Specifically, we consider that the mobilities are functions of the film height and the separation distance. In summary, our model is valid for liquid bridge formation between two identical particles coated with thin continuous films (i.e., an initial relative film height of less than 10% of the particle radius).

We observed that our results obtained from the DNS are independent of the Reynolds number, as well as the density ratio between the liquid coating the particles and the ambient gas. This suggests that our model is applicable to a wide range of gas-particle systems involving wet particulate systems.

However, our simulation study indicates that grid refinement plays an important role in the final stages of film flow where the film ruptures. To get a precise model for the filling process at long times, as well as to correctly predict film rupture, it is essential to use a fine enough computational mesh in the simulations (i.e., the dimensionless grid resolution Δh should be 0.12 or smaller). This clearly limited the current study to axisymmetric configurations. Hence, our study is only a step forward to better understand the equilibration of liquid on particles and in liquid bridged in a particle bed. Still work needs to be done in the future, specifically, it would be interesting to

- experimentally support the observed film rupturing event for long times,
- investigate the wetting of initially completely dry particle, and particles that have a complex morphology,
- quantify the effect of particle relative motion on the liquid bridge formation process.

Acknowledgments

We acknowledge the funding of the FWF through project P23617, and we gratefully acknowledge support from NAWI Graz by providing access to dcluster.tugraz.at. The authors would like to thank Ben Freireich (DOW Chemicals) for fruitful discussions on time scales associated with wet particle collisions, and the anonymous reviewers for their valuable comments.

Notation

Latin symbols

a_i = dimensionless filling rate parameter, –
Ca = capillary number, –
d_p = particle diameter, m
$\vec{F}_{\text{vis}}$ = viscous force acting on the particle, kg · m/s^2
$\vec{F}_{\text{cap}}$ = capillary force acting on the particle, kg · m/s^2
g = gravity, m/s^2
h_0 = average initial film height of the particle pair, m
h_i = initial film height of particle i, m
$h_{\text{cyl},i}$ = the height of the red shade cylinder on particle i, m
$L_{p,0}$ = reference volume of liquid on the particle, m^3
$L_{p,i}$ = volume of liquid present on the particle i, m^3
m = mass of the particle, kg
$\mathbf{n}_{\text{ij}}$ = unit normal vector, –
Oh = Ohnesorge number, –
P = pressure, Pa
P_{ref} = reference pressure, Pa
p_s = pressure at the particle surfaces, Pa
p_{V_b} = pressure at the liquid bridge, Pa
R = particle radius, m
R_{cyl} = radius of the initial cylinder region, m
R_{curve} = radius of curvature of the liquid bridge surface, m
Re = reynolds number, –
S = half separation distance between particles, m
t = time, s
t_{acc} = acceleration time scale, s
t_{cross} = film crossing time scale, s
t_{relax} = particle relation time, s
t_{ref} = reference time scale, s
u_{ref} = reference fluid velocity, m · s
u_{rel} = relative particle-particle velocity, m/s
U = fluid velocity, m/s
V_b = liquid bridge volume, m^3
$V_{b,0}$ = initial bridge volume, m^3
$V_{b,g,I}$ = geometry bridge volume: type I, m^3
$V_{b,g,II}$ = geometry bridge volume: type II, m^3
$V_{b,i,I}$ = integration volume of the red framed region in Figure 4b, m^3
$V_{\text{cap},i}$ = the cavity volume of particle, m^3
V_{overLap} = the displaced volume of liquid of the overlap region, m^3
DIM = direct integration method
DNS = direct numerical simulation
MFB = micro force balance
YLE = Young-Laplace equation

Greek symbols

α = phase fraction indicator, –
$\beta_{cyl,i}$ = initial filling angle on particle i that cause by geometry bride, rad
Δt = time step, s
Δx = grid spacing, m
Δh = dimensionless grid spacing by initial film height, –
ϕ_p = particle volume fraction, –
ϕ_{mi} = fraction of liquid on particle i that is mobile to flow into the bridge, –
μ_l = dynamic viscosity of liquid, kg m^{-1} s^{-1}
μ_g = dynamic viscosity of ambient gas, kg m^{-1} s^{-1}
ρ_l = density of the liquid, kg m^{-3}
ρ_g = density of the ambient gas, kg m^{-3}
ρ_p = density of the particles, kg m^{-3}
σ = surface tension, kg s^{-2}

Superscripts

$+$ = dimensionless quantity
i = particle index
norm = normal direction
tang = tangential direction
t = terminal
w = water
gly = glycerine
P = particle
ref = reference quantity

Literature Cited

1. Toschkoff G, Khinast JG. Mathematical modeling of the coating process. *Int J Pharm*. 2013;457(2):407–422. doi:10.1016/j.ijpharm.2013.08.022.
2. Darabi P, Pougatch K, Salcudean M, Grecov D. A novel coalescence model for binary collision of identical wet particles. *Chem Eng Sci*. 2009;64:1868–1876.
3. Scheel M, Seemann R, Brinkmann M, Di Michiel M, Sheppard A, Breidenbach B, Herminghaus S. Morphological clues to wet granular pile stability. *Nat Mater*. 2008;7:189–193. doi:10.1038/nmat2117.
4. Orr FM, Scriven LE, Rivas AP. Pendular rings between solids: meniscus properties and capillary force. *J Fluid Mech*. 1975;67(04): 723. doi:10.1017/S0022112075000572.
5. Darabi P, Li T, Pougatch K, Salcudean M, Grecov D. Modeling the evolution and rupture of stretching pendular liquid bridges. *Chem Eng Sci*. 2010;65:4472–4483. doi:10.1016/j.ces.2010.04.003.
6. Dodds S, Carvalho M, Kumar S. Stretching liquid bridges with moving contact lines: the role of inertia. *Phys Fluids*. 2011;23. doi: 10.1063/1.3623427.
7. Dodds S, Carvalho MS, Kumar S. The dynamics of three-dimensional liquid bridges with pinned and moving contact lines. *J Fluid Mech*. 2012;707:521–540. doi:10.1017/jfm.2012.296.
8. Pepin X, Rossetti D, Iveson S, Simons S. Modeling the evolution and rupture of pendular liquid bridges in the presence of large wetting hysteresis. *J Colloid Interface Sci*. 2000;232(2):289–297. doi: 10.1006/jcis.2000.7182.
9. Rossetti D, Simons SJR. A microscale investigation of liquid bridges in the spherical agglomeration process. *Powder Technol*. 2003; 130(1–3):49–55. doi:10.1016/S0032-5910(02)00225-5.
10. Herminghaus S. Dynamics of wet granular matter. *Adv Phys*. 2005; 54(3):221–261. doi:10.1080/00018730500167855.
11. Haines WB. Studies in the physical properties of soils: II. A note on the cohesion developed by capillary forces in an ideal soil1. *J Agric Sci*. 1925;15:529–535. doi:http://dx.doi.org/10.1017/S0021859600082460.
12. Fisher R. A. On the capillary forces in an ideal soil: correction of formulae given by WB haines. *J Agric Sci*. 1926;16:492–505. doi: http://dx.doi.org/10.1017/S0021859600007838.
13. Mehrotra VP, Sastry KVS. Pendular bond strength between unequal-sized spherical particles. *Powder Technol*. 1980;25:203–214.
14. Pitois O, Moucheront P, Chateau X. Liquid bridge between two moving spheres: an experimental study of viscosity effects. *J Colloid Interface Sci*. 2000;231:26–31. doi:10.1006/jcis.2000.7096.
15. McLaughlin LJ, Rhodes MJ. Prediction of fluidized bed behaviour in the presence of liquid bridges. *Powder Technol*. 2001;114:213–223. doi:10.1016/S0032-5910(00)00325-9.
16. Grof Z, Lawrence CJ, Stepánek F. The strength of liquid bridges in random granular materials. *J Colloid Interface Sci*. 2008;319(1):182–192. doi:10.1016/j.jcis.2007.11.055.
17. Rabinovich YI, Esayanur MS, Moudgil BM. Capillary forces between two spheres with a fixed volume liquid bridge: theory and experiment. *Langmuir*. 2005;21:10992–10997. doi:10.1021/la0517639.
18. Wei Z, Zhao Y-P. Growth of liquid bridge in AFM. *J Phys D Appl Phys*. 2007;40:4368–4375. doi:10.1088/0022-3727/40/14/036.
19. Muguruma Y, Tanaka T, Tsuji Y. Numerical simulation of particulate flow with liquid bridge between particles (simulation of centrifugal tumbling granulator). *Powder Technol*. 2000;109:49–57. doi: 10.1016/S0032-5910(99)00226-0.
20. Shi D, Vargas WL, McCarthy JJ. Heat transfer in rotary kilns with interstitial gases. *Chem Eng Sci*. 2008;63(18):4506–4516. doi: 10.1016/j.ces.2008.06.006.
21. De Bisschop FR., Rigole WJ. A physical model for liquid capillary bridges between adsorptive solid spheres: the nodoid of plateau. *J Colloid Interface Sci*. 1982;88:117–128. doi:10.1016/0021-9797(82)90161-8.
22. Chen Y, Zhao Y, Gao H, Zheng J. Liquid bridge force between two unequal-sized spheres or a sphere and a plane. *Particuology*. 2011;9: 374–380. doi:10.1016/j.partic.2010.11.006.
23. Davis RH, Rager DA, Good BT. Elastohydrodynamic rebound of spheres from coated surfaces. *J Fluid Mech*. 2002;468:107–119. doi: 10.1017/S0022112002001489.
24. Donahue CM, Hrenya CM, Davis RH. Stokes's cradle: Newton's cradle with liquid coating. *Phys Rev Lett*. 2010;105(3). doi:10.1103/PhysRevLett.105.034501.
25. Li X, Hunt ML, Colonius T. A contact model for normal immersed collisions between a particle and a wall. *J Fluid Mech*. 2012;691: 123–145. doi:10.1017/jfm.2011.461.
26. Gondret P, Lance M, Petit L. Bouncing motion of spherical particles in fluids. *Phys Fluids*. 2002;14(2):643–652. doi:10.1063/1.1427920.
27. Gollwitzer F, Rehberg I, Kruelle CA, Huang K. Coefficient of restitution for wet particles. *Phys Rev E Stat Nonlinear, Soft Matter Phys*. 2012;86(1):1–10. doi:10.1103/PhysRevE.86.011303.
28. Sutkar VS, Deen NG, Johan TP, Kuiper JAM, Salikov V, Cruger B, Antonyuk S, Heinrich S. A novel approach to determine wet restitution coefficients through a unified correlation and energy analysis. *AIChE J*. 2015;61:769–779. doi:10.1002/aic.
29. Kantak AA, Hrenya MC, Davis HR. Initial rates of aggregation for dilute, granular flows of wet particles. *Phys Fluids*. 2009;21(2). doi: 10.1063/1.3070830.
30. Yang F. Interaction law for a collision between two solid particles in a viscous liquid. 2006;2006.
31. Štěpánek F, Ansari MA. Computer simulation of granule microstructure formation. *Chem Eng Sci*. 2005;60:4019–4029. doi:10.1016/j.ces.2005.02.030.
32. Lian G, Thornton C, Adams MJ. A theoretical study of the liquid bridge forces between two rigid spherical bodies. *J Colloid Interface Sci*. 1993;161:138–147. doi:http://dx.doi.org/10.1006/jcis.1993.1452.
33. Erle MA, Dyson DC, Morrow NR. Liquid bridges between cylinders, in a torus, and between spheres. *AIChE J*. 1971;17:115–121. doi: 10.1002/aic.690170125.
34. Mikami T, Kamiya H, Horio M. Numerical simulation of cohesive powder behavior in a fluidized bed. *Chem Eng Sci*. 1998;53:1927–1940. doi:10.1016/S0009-2509(97)00325-4.
35. Willett CD, Adams MJ, Johnson SA, Seville JPK. Capillary bridges between two spherical bodies. *Langmuir*. 2000;16:9396–9405. doi: 10.1021/la000657y.
36. Harireche O, Faramarzi A, Alani AM. A toroidal approximation of capillary forces in polydisperse granular assemblies. *Granul Matter*. 2013;15(5):573–581. doi:10.1007/s10035-013-0425-9.
37. Simons SJR, Seville JPK, Adams MJ. An analysis of the rupture energy of pendular liquid bridges. *Chem Eng Sci*. 1994;49(14):2331–2339. doi:10.1016/0009-2509(94)E0050-Z.
38. Mazzone DN, Tardos GI, Pfeffer, R. The behavior of liquid bridge between two relatively moving particles. *Powder Technol*. 1987;51: 71–83.
39. Eggers J, Dupont TF. Drop formation in a one-dimensional approximation of the Navier-Stokes equation. *J Fluid Mech*. 1994;262:205–221. doi:10.1017/S0022112094000480.
40. Papageorgiou DT. On the breakup of viscous liquid threads. *Phys Fluids*. 1995;7(7):1529. doi:10.1063/1.868540.
41. Zhang X, Padgett RS, Basaran OA. Nonlinear deformation and breakup of stretching liquid bridges. *J Fluid Mech*. 1996;329:207. doi:10.1017/S0022112096008907.

42. Vega EJ, Montanero JM, Herrada MA., Ferrera C. Dynamics of an axisymmetric liquid bridge close to the minimum-volume stability limit. *Phys Rev E*. 2014;90(1):013015. doi:10.1103/PhysRevE.90.013015.
43. Wu M, Khinast J, Radl S. Direct simulation of film flow on spheres to investigate liquid bridge. In: *2014 AICHE Annual Meeting, November 16*. Atlanta, Vereinigte Staaten (USA); 2014.
44. Easo LA, Kumar R, Ren R, Carl R. Numerical study of the formation of a liquid bridge between two spheres with uniform film thickness. In: *2014 AICHE Annual Meeting, November 18*. 2014.
45. Radl S, Khinast JG, Sundaresan S. On the filling rate of a liquid bridge between wet particles. In: *2013 AICHE Annual Meeting, November 03–08*. San Francisco, Vereinigte Staaten (USA); 2013.
46. Shi D, McCarthy JJ. Numerical simulation of liquid transfer between particles. *Powder Technol*. 2008;184:64–75. doi:10.1016/j.powtec.2007.08.011.
47. Mohan B, Kloss C, Khinast J, Radl S. Regimes of liquid transport through sheared beds of inertial smooth particles. *Powder Technol*. 2014;264:377–395. doi:10.1016/j.powtec.2014.05.045.
48. Deshpande SS, Anumolu L, Trujillo MF. Evaluating the performance of the two-phase flow solver interFoam. *Comput Sci Discov*. 2012;5(1):014016. doi:10.1088/1749-4699/5/1/014016.
49. Eddi a., Winkels KG, Snoeijer JH. Short time dynamics of viscous drop spreading. *Phys Fluids*. 2013;25(1):013102. doi:10.1063/1.4788693.
50. Radl S, Sundaresan S. A drag model for filtered Euler-Lagrange simulations of clustered gas-particle suspensions. *Chem Eng Sci*. 2014;117:416–425. doi:10.1016/j.ces.2014.07.011.
51. Kloss C, Goniva C, Hager A, Amberger S, Pirker S. Models, algorithms and validation for opensource DEM and CFD-DEM. *Prog Comput Fluid Dyn*. *2012*;12:140–152. doi:10.1504/PCFD.2012.047457.

Appendix A: Analytical Solution for a Two-Particle System

The mass balance equations detailed in the manuscript can be normalized and written for the simplest case of a two-particle collision:

$$\frac{dL_{p1}^{+}}{dt^{+}} = -a_i\left(L_{p1}^{+}\phi_{m1} - \frac{V_b^{+}}{2}\right) \tag{A1}$$

$$\frac{dL_{p2}^{+}}{dt^{+}} = -a_i\left(L_{p2}^{+}\phi_{m2} - \frac{V_b^{+}}{2}\right) \tag{A2}$$

$$\frac{dV_b^{+}}{dt^{+}} = -\left(\frac{dL_{p1}^{+}}{dt^{+}} + \frac{dL_{p2}^{+}}{dt^{+}}\right) \tag{A3}$$

The initial conditions are:

$$V_b^{+}|_{t=0} = V_{b,0}^{+},\ L_{p1}^{+}|_{t=0} = L_{p1,0}^{+},\ L_{p2}^{+}|_{t=0} = L_{p2,0}^{+} \tag{A4}$$

Exploiting the total mass balance, that is, Eq. A3, assuming that a_i is a constant for the pair of particles, and taking the time derivatives of the above equations, we arrive at:

$$\frac{dL_{p1}^{+\prime}}{dt^{+}} = -a_i\left(\left(\phi_{m1} + \frac{1}{2}\right)L_{p1}^{+\prime} + \frac{1}{2}L_{p2}^{+\prime}\right) \tag{A5}$$

$$\frac{dL_{p2}^{+\prime}}{dt^{+}} = -a_i\left(\left(\phi_{m2} + \frac{1}{2}\right)L_{p2}^{+\prime} + \frac{1}{2}L_{p1}^{+\prime}\right) \tag{A6}$$

where $L_{p1}^{+\prime} = \frac{dL_{p1}^{+}}{dt^{+}}$, $L_{p2}^{+\prime} = \frac{dL_{p2}^{+}}{dt^{+}}$. By rearranging Eq. A5, we now obtain an expression of $L_{p2}^{+\prime}$ in terms of $L_{p1}^{+\prime}$

$$L_{p2}^{+\prime} = -2\left(\frac{1}{a_i}\frac{dL_{p1}^{+\prime}}{dt^{+}} + \left(\phi_{m1} + \frac{1}{2}\right)L_{p1}^{+\prime}\right) \tag{A7}$$

We then substitute Eq. A7 into Eq. A6, to arrive at the following second-order constant coefficient homogeneous linear differential equation in for $L_{p1}^{+\prime}$,

$$\frac{2}{a_i}\frac{d^2L_{p1}^{+\prime}}{dt^{+2}} + 2(\phi_{m1}+\phi_{m2}+1)\frac{dL_{p1}^{+\prime}}{dt^{+}} + a_i(2\phi_{m1}\phi_{m2}+\phi_{m1}+\phi_{m2})L_{p1}^{+\prime} = 0 \tag{A8}$$

Using the Ansatz

$$L_{p1}^{+\prime} \equiv e^{rt^{+}} \tag{A9}$$

We obtain the characteristic equation

$$\frac{2}{a_i}r^2e^{rt^{+}} + 2(\phi_{m1}+\phi_{m2}+1)re^{rt^{+}} + a_i(2\phi_{m1}\phi_{m2}+\phi_{m1}+\phi_{m2})e^{rt^{+}} = 0 \tag{A10}$$

which has the real-numbered roots:

$$r_1 = \frac{-a_i\left(\phi_{m1}+\phi_{m2}+1+\sqrt{(\phi_{m1}-\phi_{m2})^2+1}\right)}{2} \tag{A11}$$

$$r_2 = \frac{-a_i\left(\phi_{m1}+\phi_{m2}+1-\sqrt{(\phi_{m1}-\phi_{m2})^2+1}\right)}{2} \tag{A12}$$

Hence, the general solution for Eq. A8 is given by

$$\frac{L_{p1}^{+}}{dt^{+}} = C_1e^{r_1t^{+}} + C_2e^{r_2t^{+}}, \tag{A13}$$

$$\frac{L_{p2}^{+}}{dt^{+}} = -2\left(\frac{1}{a_i}\left(C_1r_1e^{r_1t^{+}} + C_2r_2e^{r_2t^{+}}\right) + \left(\phi_{m1}+\frac{1}{2}\right)\left(C_1e^{r_1t^{+}} + C_2e^{r_2t^{+}}\right)\right) \tag{A14}$$

and

$$\frac{dV_b^{+}}{dt^{+}} = \left(\frac{2r_1}{a_i} + 2\phi_{m1}\right)C_1e^{r_1t^{+}} + \left(\frac{2r_2}{a_i} + 2\phi_{m1}\right)C_2e^{r_2t^{+}} \tag{A15}$$

Using the initial conditions, that is, $V_b^{+}|_{t=0} = V_{b,0}^{+}$, $L_{p1}^{+}|_{t=0} = L_{p1,0}^{+}$, and $L_{p2}^{+}|_{t=0} = L_{p2,0}^{+}$, and after rearrangement we arrive at:

$$C_1 = \frac{-a_i^2\phi_{m2}L_{p2,0}^{+} - \left(2a_ir_2\phi_{m1} + 2a_i^2\phi_{m1}^2 + a^2\phi_{m1}\right)L_{p1,0}^{+}}{2(r_2-r_1)} + \frac{\left(a_i^2\phi_{m1} + a_i^2 + a_ir_2\right)V_{b,0}^{+}}{2(r_2-r_1)} \tag{A16}$$

$$C_2 = \frac{a_i^2\phi_{m2}L_{p2,0}^{+} + \left(2a_ir_1\phi_{m1} + a_i^2\phi_{m1} + 2a_i^2\phi_{m1}^2\right)L_{p1,0}^{+} - \left(a_ir + a_i^2\phi_{m1} + a_i^2\right)V_{b,0}^{+}}{2(r_2-r_1)} \tag{A17}$$

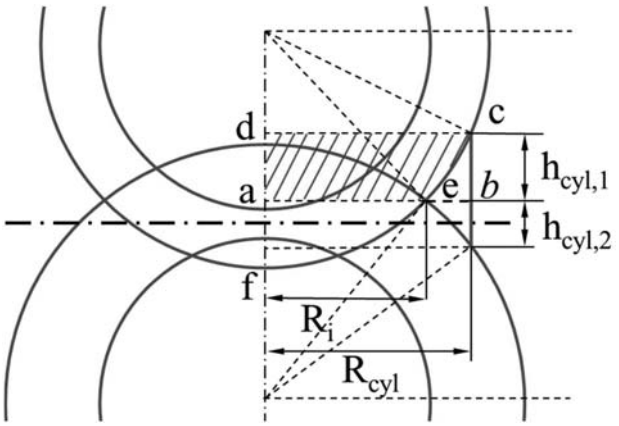

Figure B1. Sketch illustrating the unknown variables in the calculation of the geometrical bridge volume type II.

[Color figure can be viewed in the online issue, which is available at wileyonlinelibrary.com.]

by integration of Eq. A15, as well as using the initial condition for the bridge volume, we obtain

$$V_b^+ = V_{b,0}^+ + C_1 \frac{\frac{2r_1}{a_i} + 2\phi_{m1}}{r_1}\left(e^{r_1 t^+} - 1\right) + C_2 \frac{\frac{2r_2}{a_i} + 2\phi_{m1}}{r_2}\left(e^{r_2 t^+} - 1\right) \tag{A18}$$

Similarly, we obtain the following equations for the dimensionless liquid content on particle 1 and particle 2:

$$L_{p1}^+ = L_{p1,0}^+ + \frac{C_1}{r_1}\left(e^{r_1 t^+} - 1\right) + \frac{C_2}{r_2}\left(e^{r_2 t^+} - 1\right) \tag{A19}$$

$$L_{p2}^+ = L_{p2,0}^+ - C_1 \frac{\frac{2r_1}{a_i} + 2\phi_{m1} + 1}{r_1}\left(e^{r_1 t^+} - 1\right) - C_2 \frac{\frac{2r_2}{a_i} + 2\phi_{m1} + 1}{r_2}\left(e^{r_2 t^+} - 1\right) \tag{A20}$$

Appendix B: Details on the Geometrical Bridge Volume Type II

The key to calculate the volume of liquid bridges of type II is the calculation of the radius R_{cyl} of the compensation cylinder region. The known parameters, as shown in Figure 1 (panel a), are the particle radius R, the initial film heights h_1 and h_2, and the half separation between particles S. Once two particles have been fixed in space, the liquid in the overlap regions of the liquid films (i.e., the red and green shaded regions in Figure 1, panel b) is displaced and flows into a ring-shaped region (i.e., red solid area in Figure 1, panel b). One can compute the volume of the ring-shaped region as follows:

First, the overlap liquid volume that is contributed by particle 1 (i.e., the green shaded area in Figure 1, panel b) and particle 2 (i.e., the red shaded area in Figure 1, panel b) can be computed from:

$$V_{overLap} = \frac{1}{24}\frac{1}{R+S}\left(\pi\left(12h_1^2R^2 - 24h_1^2S^2 + 4Rh_1^3 + 16h_1^3S - 3h_1^4 - 48R^2h_1S - 48Rh_1S^2 + 96R^2S^2 + 128RS^3 + 32S^4 + 12R^2h_2^2 - 24h_2^2S^2 + 4Rh_2^3 + 16h_2^3S - 3h_2^4 - 48R^2h_2S - 48Rh_2S^2\right)\right) \tag{B1}$$

Second, the intersection radius R_i can be calculated using Eq. B2 as illustrated in Figure B1B1.

$$\sqrt{(R+h_1)^2 - R_i^2} + \sqrt{(R+h_2)^2 - R_i^2} = 2(R+S) \tag{B2}$$

Third, the ring-shaped region is divided into two sub-regions, which have the heights $h_{cyl,1}$ and $h_{cyl,2}$ as sketched in Figure B1. The ring-shaped sub-region 1 has the volume $V_{cyl,1} = V_{abcd} - V_{aecd}$, where $V_{aecd} = V_{dcf} - V_{cap,aef}$. The cap height is $h_{af} = R + h_1 - \sqrt{(R+h_1)^2 - R_i^2}$, and thus the cap volume is $V_{cap,aef} = \frac{\pi h_{af}}{6}\left(3R_i^2 + h_{af}^2\right)$. The liquid volume in sub-region 2, that is, $V_{cyl,2}$ can be computed in the same fashion.

Finally, we sum up the two sub-regions, and use the known volume of the displaced liquid, that is, $V_{overLap}$, to arrive at the following expression involving the unknowns R_{cyl}, h_1, h_2, S, and R:

$$V_{overLap} = V_{cyl} = V_{cyl,1} + V_{cyl,2} = f\left(R_{cyl}, h_1, h_2, S, R\right) \tag{B3}$$

This expression cannot be solve directly to obtain R_{cyl}, however, one can solve it numerically using, for example, a Newton algorithm. Once R_{cyl} is known, we can calculate the geometrical bridge volume based on the contribution from each particle i and as illustrated in shown in Figure 4 (panel b):

$$\beta_{cyl,i} = \arcsin\left(\frac{R_{cyl}}{R+h_i}\right) \tag{B4}$$

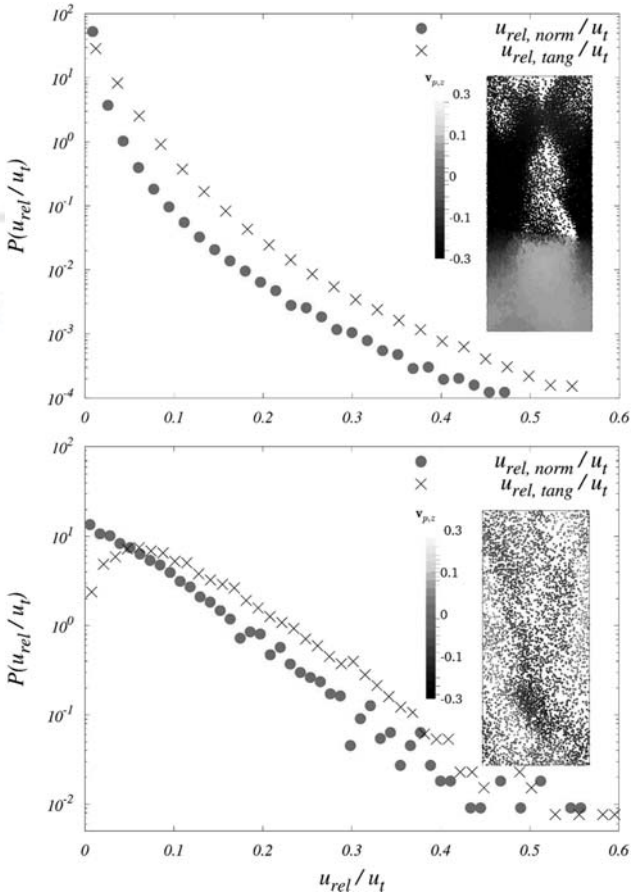

Figure C1. Distribution of the relative particle velocity at impact in a dilute (bottom panel; $\phi_p = 0.05$) and dense (top panel; $\phi_p = 0.30$) cloud of freely sedimenting particles (the inserts illustrate individual-particle velocities in the vertical direction).

[Color figure can be viewed in the online issue, which is available at wileyonlinelibrary.com.]

$$h_{\mathrm{cyl},i} = (R+S) - (R+h_i)cos\beta_{\mathrm{cyl},i} \tag{B5}$$

$$V_{\mathrm{cap},i} = \frac{\pi R^3}{3}(1-\cos\beta_{\mathrm{cyl},i})^2(2+\cos\beta_{\mathrm{cyl},i}) \tag{B6}$$

$$V_{\mathrm{b},i,\mathrm{I}} = \pi R_{\mathrm{cyl}}^2 h_{\mathrm{cyl},i} + \frac{1}{3}\pi h_i \cos\beta_{\mathrm{cyl},i}\sin^2\beta_{\mathrm{cyl},i} \left(R^2 + (R+h_i)^2 + R(R+h_i)\right) \tag{B7}$$

$$V_{\mathrm{b,g,II},i} = V_{\mathrm{b},i,\mathrm{I}} - V_{\mathrm{cap},i} \tag{B8}$$

Appendix C: Relative Particle Velocity at Impact in a Sedimenting Suspension

We summarize statistics of the relative particle speed at impact in a fully periodic domain using soft-sphere Euler-Lagrange simulations using the code CFDEM® (Kloss et al.[51]). Particles were allow to sediment under the action of gravity, while their weight (and that of the surrounding gas) was balanced by a pressure gradient, similar to our previous work (see, Radl and Sundaresan[50]). Also numerical parameters and drag models were identical to this previous work (a dimensionless grid resolution of $\Delta x/(2R) = 3$, as a domain size of 53 $\times$ 53 $\times$ 213 d_p was used). The statistics reported below were collected by sampling impact velocities over a sufficiently long time, that is, 40 times the particle relaxation time $t_{\mathrm{relax}} = u_t^2/g$. Note that the particles were initialized homogeneously distributed in the computational domain, and that a statistical steady state was reached after ca. $5t_{\mathrm{relax}}$.

Manuscript received June 12, 2015, and revision received Jan. 22, 2016.

AQ1: Please provide page range for Refs. 6, 24, and 29.

AQ2: Please provide complete publication details for Ref. 30.

AQ3: Please provide location details for Ref. 44.

AQ4: Please confirm that given names (red) and surnames/family names (green) have been identified correctly.

Ref. 6. Dodds S, Carvalho M, Kumar S. Stretching liquid bridges with moving contact lines: The role of inertia. Phys Fluids. 2011;23(9):092101. doi:10.1063/1.3623427.

Ref 24. Donahue CM, Hrenya CM, Davis RH. Stokes's cradle: Newton's cradle with liquid coating. Phys Rev Lett. 2010;105(3):034501. doi: 10.1103/PhysRevLett.105.034501.

Ref 29. Kantak AA, Hrenya MC, Davis HR. Initial rates of aggregation for dilute, granular flows of wet particles. Phys Fluids. 2009;21(2):023301. doi: 10.1063/1.3070830.

Ref. 30. Yang F. Interaction Law for a Collision Between Two Solid Particles in a Viscous Liquid. (Ph D) Thesis Calif Inst Technol. 2006. doi: etd-05262006-120244.

Ref. 44. Easo LA, Kumar R, Ren R, Carl R. Numerical Study of the Formation of a Liquid Bridge Between Two Spheres with Uniform Film Thickness. In: 2014 AICHE Annual Meeting, November 18. Atlanta; 2014.